

# Text-Based Reasoning About Vector Graphics

Zhenhailong Wang<sup>1</sup>, Joy Hsu<sup>2</sup>, Xingyao Wang<sup>1</sup>, Kuan-Hao Huang<sup>1</sup>, Manling Li<sup>2</sup>,  
Jiajun Wu<sup>2</sup>, Heng Ji<sup>1</sup>

<sup>1</sup>University of Illinois Urbana-Champaign, <sup>2</sup>Stanford University

{wangz3,xingyao6,khuang,hengji}@illinois.edu

{joycj,manlingl}@stanford.edu, jiajunwu@cs.stanford.edu

## Abstract

Despite their successes in general vision-language benchmarks, current large multimodal models (LMMs) still struggle with seemingly straightforward reasoning tasks that require precise perception of low-level visual details, such as comparing line lengths or solving simple mazes. In particular, this failure mode persists in question-answering tasks about vector graphics—images composed purely of 2D objects and shapes. To address this challenge, we propose the **Visually Descriptive Language Model (VDLM)**, which performs *text-based* reasoning about vector graphics. VDLM leverages Scalable Vector Graphics (SVG) for a more precise visual description and first uses an off-the-shelf raster-to-SVG algorithm for encoding. Since existing language models cannot understand raw SVGs in a zero-shot setting, VDLM then bridges SVG with pretrained language models through a newly introduced intermediate symbolic representation, **Primal Visual Description (PVD)**, comprising primitive attributes (e.g., *shape*, *position*, *measurement*) with their corresponding predicted values. PVD is task-agnostic and represents visual primitives that are universal across all vector graphics. It can be learned with procedurally generated  $\langle \text{SVG}, \text{PVD} \rangle$  pairs and also enables the direct use of LLMs for generalization to complex reasoning tasks. By casting an image to a text-based representation, we can leverage the power of language models to learn alignment from SVG to visual primitives and generalize to unseen question-answering tasks. Empirical results show that VDLM achieves stronger zero-shot performance compared to state-of-the-art LMMs, such as GPT-4V, in various low-level multimodal perception and reasoning tasks on vector graphics. We additionally present extensive analyses on VDLM’s performance, demonstrating that our framework offers better interpretability due to its disentangled perception and reasoning processes. Project page: <https://mikewangzhl.github.io/VDLM/>

## 1 Introduction

In recent years, large multimodal models (LMMs) (OpenAI, 2023b; Anil et al., 2023; Liu et al., 2023b; Chen et al., 2023b; Bai et al., 2023) have achieved impressive performance across a broad spectrum of general vision-language benchmarks (Goyal et al., 2017; Fu et al., 2023; Liu et al., 2023d; Yu et al., 2023; Li et al., 2023a). However, these monolithic LMMs still struggle with seemingly simple tasks that require precise perception of low-level visual details (Guan et al., 2024). For example, they often fail to accurately compare the lengths of two line segments, identify the spatial relationships between two shapes, or navigate through  $2 \times 2$  mazes. In particular, we empirically observe that LMMs extensively exhibit this failure mode in **vector graphics**, which are images composed purely of 2D objects and shapes, devoid of any camera viewpoint (see Figure 1 for an example).

To achieve precise visual perception for vector graphics, we explore the alternative path of *text-based* reasoning, which allows us to leverage large language models. To do so, we first vectorize a rasterized image using the Scalable Vector Graphics (SVG) representation, which

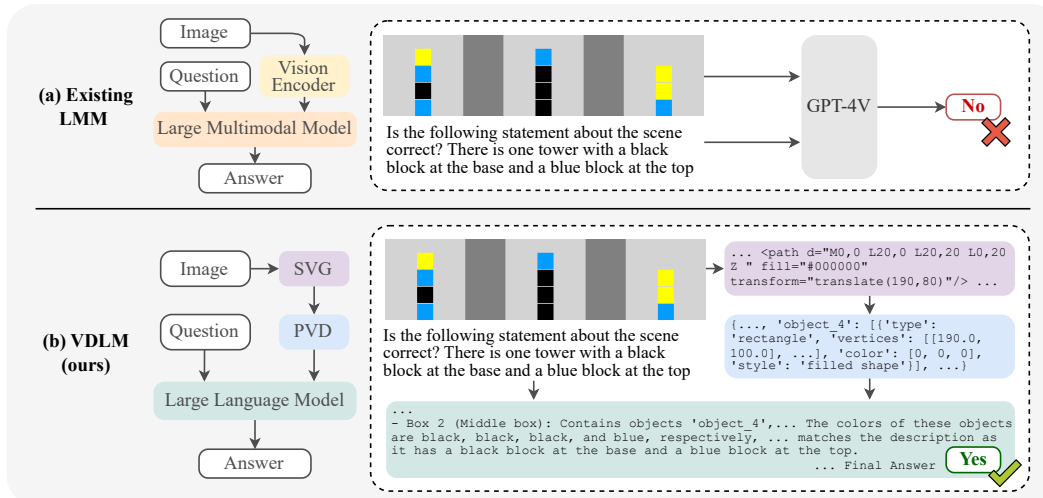


Figure 1: Comparison of existing monolithic LMMs and VDLM. Prior works rely on pre-trained vision encoders for perception, which fall short of accurately capturing low-level visual details in vector graphics. VDLM enables precise visual reasoning by first encoding the input image into SVG format and then learning an intermediate symbolic representation (PVD) that bridges the low-level SVG perception and high-level language reasoning.

describes a scene with “`<path/>`”s (e.g., polygons and splines) and their corresponding measurements and positions. SVG representations, by nature, are unbiased towards high-level features and can capture low-level visual details in text. The vectorization process itself is straightforward for vector graphics and can be faithfully accomplished with an off-the-shelf, rule-based raster-to-vector algorithm.

However, the SVG representation, though text-based, is insufficient for reasoning with language models: our preliminary experiments (§A) demonstrate that existing large language models (LLMs) are unable to understand raw SVGs in zero-shot settings, and additionally, finetuning a model to reason about raw SVGs can be inefficient and infeasible without corresponding task-specific annotations. To address this challenge, we propose training a language model to align extracted SVG paths to an intermediate symbolic representation, from which we can directly leverage an inference-only LLM for reasoning. To this end, we introduce **Primal Visual Description (PVD)**, which bridges the low-level SVG representation and the high-level language space required for reasoning in vector graphics. Specifically, we train an LLM-based (Jiang et al., 2023) SVG-to-PVD model, which transforms the raw SVG paths into a set of primitive attributes (e.g., *shape*, *position*) with corresponding predicted values (e.g., *rectangle*, *pixel coordinates of the vertices*). See Figure 1 in the blue box for an example. Notably, the PVD representation contains primitive attributes that are *universal* across vector graphics, can be learned with procedurally generated  $\langle \text{SVG}, \text{PVD} \rangle$  pairs for training, and enables direct usage of LLMs for generalization to complex reasoning tasks.

Comprising SVG-based image representations and primitive-level abstractions, we present our method, the **Visually Descriptive Language Model (VDLM)**, a text-based visual reasoning framework for vector graphics. VDLM has three components: a rule-based visual encoder that converts images to SVG to capture precise visual features, a learned language model that translates SVG to PVD, and an inference-only LLM that conducts zero-shot reasoning about downstream tasks with the PVD representation. Our learned language model is trained with 160K procedurally generated  $\langle \text{SVG}, \text{PVD} \rangle$  pairs and produces visually descriptive scene representations that generalize across different domains of vector graphics. By first casting the image into a text-based representation, VDLM is able to take advantage of language models to learn the alignment of low-level SVG paths with visual primitives, as well as to generalize to unseen reasoning tasks.

Experimental results demonstrate that VDLM achieves strong zero-shot performance in various visual reasoning tasks, outperforming LLaVA-v1.5 (Liu et al., 2023a), GPT-4V (Ope-

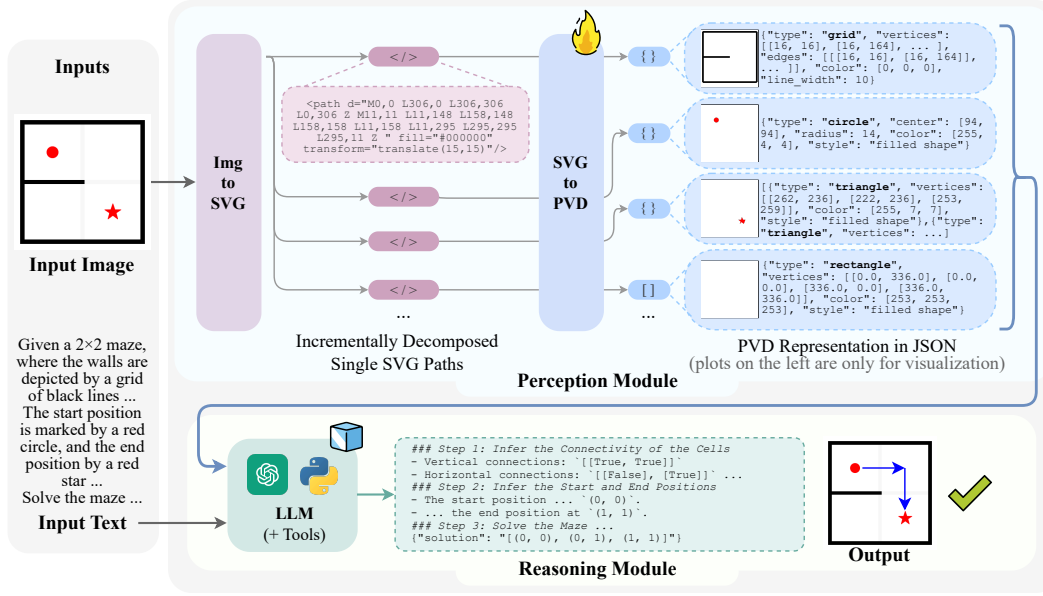


Figure 2: A walkthrough example of VDLM during inference. VDLM first extracts single SVG paths from the input image, then transforms them into PVD descriptions using a learned language model. Lastly, it feeds the PVD perception results to an inference-only LLM for reasoning. Note that although “star” (★) is not directly in the ontology of PVD primitives (see Figure 3), the SVG-to-PVD model can approximate the “star” using a composition of two triangles (★). A strong off-the-shelf LLM, e.g., GPT-4 (OpenAI, 2023a), can correctly infer that this composition corresponds to the “star”, i.e., the target end position of the maze, purely based on text-based reasoning. See Figure 13 for the full response.

nAI, 2023b), and Visual Programming approaches such as ViperGPT (Surís et al., 2023). We observe that the learned SVG-to-PVD model is capable of denoising imperfect perceptions from the SVG encoder, and that our LLM reasoning module (OpenAI, 2023a) is capable of interpreting the PVD representation based on different task instructions. VDLM also enhances interpretability through its disentangled perception and text-based reasoning processes. Moreover, we conduct an in-depth analysis of the impact of perception quality on final task performance, revealing that more accurate perception leads to improved overall performance. This underscores the strength of VDLM in capturing fine-grained visual features and enabling individual modules to enhance the performance of the entire framework.

To summarize, the key contributions of our work are threefold: First, we identify a critical failure mode of LMMs when reasoning about tasks that require precise, low-level perception in vector graphics. Second, we introduce VDLM, a visual reasoning framework that operates on text-based visual descriptions—SVG representations and learned Primal Visual Description, which enables zero-shot reasoning with an off-the-shelf LLM. Finally, we show that VDLM outperforms previous state-of-the-art LMMs; our analysis also provides insights into the perception and reasoning steps of VDLM.

## 2 VDLM Framework

We present the VDLM framework, which comprises three components. First, a rule-based perception module transforms images into SVG format, accurately capturing low-level visual details (§ 2.1). Second, a trained language model aligns SVGs with intermediate visual descriptions by mapping SVG paths to geometric shapes (§ 2.2). Third, an inference-only LLM reasons about the downstream tasks with the text-based perception results (§ 2.3). See Figure 2 for an overview of VDLM.

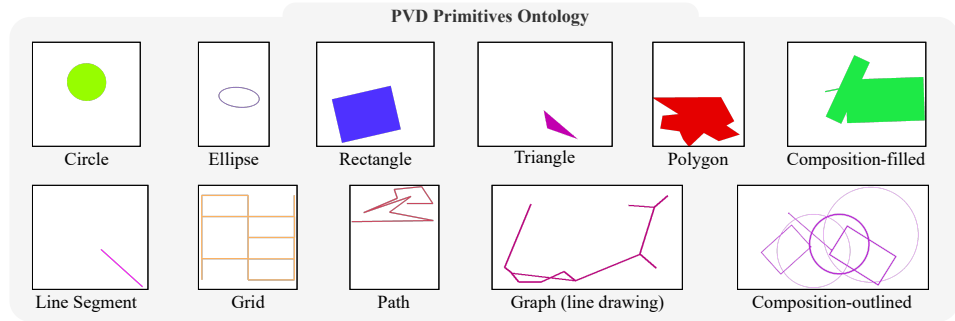


Figure 3: Ontology of the primitives in Primal Visual Description (PVD).

In this work, we focus on multimodal reasoning tasks involving vector graphics, which are images composed purely of 2D objects and shapes, without a camera viewpoint. Recent multimodal benchmarking (Yue et al., 2023; Lu et al., 2023; Huang et al., 2023) shows that, compared with natural images, current LLMs struggle with abstract images such as charts and figures more. Moreover, SVG representations are unsuitable for depicting 3D scenes or natural images due to the ineffectiveness of using 2D paths to describe lighting, shadows, and perspectives. We leave the extension to 3D objects and natural images for future work.

## 2.1 Encoding Images into SVG with Rule-based Algorithms

Prior work (Krojer et al., 2022; Tong et al., 2024) has demonstrated that, although CLIP-based (Radford et al., 2021) vision encoders are effective at capturing high-level visual semantics, they can fall short in preserving fine-grained visual details. As an alternative, we propose using a rule-based raster-to-SVG algorithm to extract an SVG representation that more accurately captures the detailed measurements. Unlike raster graphics, such as JPEG or PNG images, which represent images through a grid of pixels, SVG describes shapes, lines, and colors using mathematical expressions and paths with precise coordinates. We posit that these distinctions allow SVG representations to more faithfully describe visual scenes in vector graphics.

To empirically verify this, we conduct a suite of preliminary experiments (§ A) investigating the potential of using SVG for representing visual inputs. We find that on vector graphics tasks, fine-tuning the LLM backbone, Vicuna (Chiang et al., 2023), of an Llava-v1.5 (Liu et al., 2023a), with SVG representations consistently outperforms fine-tuning the entire Llava model with image representations. Importantly, we can leverage an off-the-shelf rule-based image-to-SVG parsing algorithm (VTracer) for converting any image into SVG without learning. This enables us to obtain an unbiased initial description of the visual input. However, we observe two key challenges (§ A.3) when working with raw SVG representation. First, off-the-shelf LLMs, e.g., GPT-4 (OpenAI, 2023a), have a limited zero-shot reasoning ability on SVG representation. Even with fine-tuning, training an LLM to directly understand raw SVG code can still be challenging. Second, fine-tuning on task-specific  $\langle$ SVG, question, answer $\rangle$  pairs limits generalization to unseen tasks and domains. We discuss our approach for extracting intermediate representations below.

## 2.2 Learning Alignment of SVG to Primal Visual Description with Language Models

**Primal Visual Description (PVD).** We propose Primal Visual Description, a higher-level scene representation that bridges low-level SVG paths to more structured primitives required for reasoning. PVD is a text-based visual description that consists of a set of primitive geometry objects, e.g., circles and line segments. Each PVD element contains the primitives' attributes (e.g., color, shape, position, size) with corresponding predicted values (e.g., blue, circle, pixel coordinates of the center, length of the radius). An example of the PVD representation in JSON is shown as follows (See Figure 12 for full definitions):

```
{"type": "circle", "center": [252, 315], "radius": 202, "color": [175, 155, 98], "style": "filled shape"}
```

Notably, the PVD is a higher level of abstraction that can be extracted from SVG, from which we can directly leverage the strong reasoning abilities of an off-the-shelf LLM to generalize across various downstream tasks. Moreover, the PVD is general enough to serve as a unified visual description across different types of images.

As shown in Figure 3, the ontology of the Primal Visual Description contains 9 primitive shape types that can be composed to cover diverse vector graphics in the wild. The primitive shapes include circles, ellipses, rectangles, triangles, polygons, line segments, grids, paths, and graphs. A path in PVD is defined as a non-intersecting polyline. Graphs and grids are defined as a set of vertices connected by a set of edges.

**Learning alignment with a language model.** We then train a language model to generate PVD outputs from SVG inputs. The input is a *single* SVG path depicting a visual concept, and the output is the predicted one or more primitives in the defined PVD ontology. During inference, given an arbitrary raster image, we first convert it into a raw SVG file, which may contain a large number of SVG paths, including unimportant noise and speckles. To denoise the raw SVG file and extract salient single SVG paths, we propose an *incremental decomposition algorithm*. Specifically, we incrementally include SVG paths while checking the difference between the partially rendered image of currently chosen paths and the fully rendered image of the original raw SVG file. We compute the summation of the absolute pixel-by-pixel difference between the two images and set an empirical threshold. If the difference after adding a new path is below this threshold, i.e., if the added path does not bring much additional visual information to the scene, we will skip that path. For the ordering of the path selection, we follow the default ordering from VTracer that heuristically places the paths with a larger area at the front. The paths that come afterward will be stacked on top of previous paths during rendering. Upon obtaining the decomposed single SVG paths, we first generate their PVD representation individually. We then aggregate the individual PVD predictions into a holistic perception of the entire image using this simple template: ["object\_0": < PVD output for path 0 >, "object\_1": < PVD output for path 1 >, ...].

Since PVD is task-agnostic, the data for training the SVG-to-PVD model can be procedurally generated without human annotation. We develop a data generator leveraging PIL.ImageDraw\* and VTracer, which creates a large-scale (SVG, PVD) paired dataset containing randomly generated primitives. In some real-world tasks, such as geometry problems, multiple primitive shapes with the same color can overlap. When converted to SVG, these shapes tend to be parsed into one merged SVG path. To enable the SVG-to-PVD model to learn to decode individual primitives from such compositional concepts, we additionally generate data instances with randomly overlapped shapes. The target PVD representation, in this context, is a list of primitive PVD JSON objects. We ensure that each generated image contains only one unicolor object, single or composed, so that the converted SVG contains a single SVG <path/>. This facilitates a language model in effectively learning the alignment between SVG and PVD.

To improve the robustness to unseen inference images, we randomize the image sizes, the positions and rotations of the shapes, as well as the styles of the shapes (filled or outlined). We additionally use two data augmentation methods, Gaussian Blur and Pixel Noise, to add variance to the training SVG paths. Our final dataset contains 160K (SVG, PVD) pairs. More details can be found in Appendix C.

We fine-tune a pretrained Mistral-7b (Jiang et al., 2023) model on the synthesized PVD 160K dataset to perform SVG-to-PVD generation. We conduct full-parameter fine-tuning for 3 epochs with a learning rate of 1e-5. The training objective is a standard Language Modeling

\*<https://pillow.readthedocs.io/en/stable/reference/ImageDraw.html>

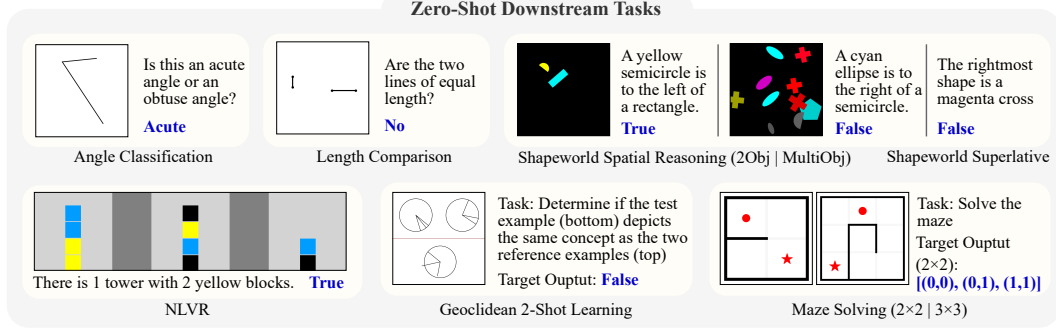


Figure 4: Our full evaluation benchmark, composed of 9 zero-shot tasks on vector graphics.

loss on the generated PVD tokens as follows:

$$\mathcal{L} = -\frac{1}{N} \sum_{i=1}^N \log P(\mathbf{d}_i | \mathbf{s}, \mathbf{d}_{0:i-1}) \quad (1)$$

where  $\mathbf{s}$  and  $\mathbf{d}$  refer to the input SVG tokens and the generated PVD tokens respectively. We use the Megatron-LLM (Cano et al., 2023) library for efficient LLM fine-tuning and the entire training process can be done in 16 hours on 4 NVIDIA A100-40GB GPUs.

### 2.3 Reasoning about Primal Visual Description with LLMs

Our visual perception modules generate a fully text-based visual description from the input vector graphics. For each downstream task, we input the perception result into the prompt along with the task-specific instructions, and then feed it into an off-the-shelf LLM for reasoning. Example prompts can be found in Figures 15-22. Additionally, we investigate augmenting LLMs with code interpreters (Yang et al., 2024; Wang et al., 2024) to assist with more challenging reasoning tasks on the PVD perception results.

A detailed execution trace from the VDLM functions is illustrated in Figure 2. We observe that a strong LLM, such as GPT-4, without any fine-tuning, can already effectively perform various types of task-specific reasoning based on our Primal Visual Description. This includes identifying higher-level concepts, computing measurements, examining spatial relations, and performing multi-step reasoning. The reasoning procedure is also more explainable and transparent compared to the output of an LMM.

## 3 Experiments

**Tasks.** We construct an evaluation benchmark that comprises 9 tasks which cover important aspects of low-level visual perception and vision-language reasoning, including measurements, spatial relations, counting, logical reasoning, and complex reasoning problems such as maze solving. The description of each task is as follows: (1) **Angle Classification:** Identify whether an angle is acute or obtuse. (2) **Length Comparison:** Determine whether two line segments are of equal length. (3-4) **Shapeworld Spatial Reasoning:** The Shapeworld (Kuhnle & Copestake, 2017) dataset on spatial relations with images containing exactly **two** objects or **multiple** objects. (5) **Shapeworld Superlative:** The Shapeworld dataset on superlative statements. (6) **NLVR:** The Natural Language for Visual Reasoning dataset (Suhr et al., 2017) which contains diverse counting, spatial reasoning, and logical reasoning queries. (7) **NLVR:** A repurposed Geoclidian (Hsu et al., 2022) dataset requiring the model to understand a compositional geometric concept with only two reference examples. (8-9) **Maze Solving:** Solve a  $2 \times 2$  or  $3 \times 3$  maze, given the starting and ending positions. Among these tasks, Angle Classification, Length Comparison, and Maze Solving were newly created by us (See Appendix F for more details). Figure 4 shows simplified input and output examples for each task. Full prompts can be found in Appendix E. For each task, we consider a zero-shot evaluation setting where the task is unseen by the models.

Tools	AC	LC	SW-S 2Obj	SW-S mObj	SW Sup	NLVR	Geo	Maze 2×2	Maze 3×3	All
Llava-v1.5-7b	-	0.53	0.49	0.48	0.55	0.35	0.53	0.50	0.00	0.00   0.38
Llava-v1.5-13b	-	0.53	0.51	0.51	0.47	0.61	0.48	0.50	0.00	0.00   0.40
GPT-4V	-	0.58	0.64	0.77	0.60	0.61	0.63	<u>0.64</u>	0.28	0.02   0.53
ViperGPT (w/ GPT-4)	CI	0.11	0.67	0.61	0.47	0.53	0.43	0.02	0.03	0.00   0.32
<b>VDLM</b> (w/ GPT-4)	-	<b>0.89</b>	<b>0.95</b>	<b>0.78</b>	<b>0.63</b>	<b>0.80</b>	<b>0.68</b>	0.63	<b>0.40</b>	<b>0.19</b>   <b>0.66</b>
<b>VDLM</b> (w/ GPT-4)	CI	0.73	0.95	0.89	0.68	0.72	<b>0.72</b>	<b>0.64</b>	<b>0.40</b>	<b>0.26</b>   <b>0.67</b>

Table 1: **Zero-shot downstream task accuracy.** Task abbreviations: AC (Angle Classification), LC (Length Comparison), SW-S-2Obj/mObj (Shapeworld Spatial Reasoning with two objects or multiple objects), SW-Sup (Shapeworld Superlative), Geo (Geoclidene 2-shot Learning). “CI” refers to Code Interpreter. Underlined scores denote the best method without an external tool. For methods utilizing interpreters, there can be instances where the final question is not generated due to code execution errors. We treat such instances as incorrect.

**Models.** We compare our work with strong baselines, including both state-of-the-art end-to-end large multimodal models (LMMs), i.e., LLaVA-v1.5 (Liu et al., 2023a), GPT-4V (OpenAI, 2023a)<sup>†</sup>, as well as visual programming agents, e.g., ViperGPT (Surís et al., 2023). ViperGPT employs an LLM to generate code, which can call external vision models, such as GLIP (Li et al., 2022) and BLIP2 (Li et al., 2023b), to process the image and generate the final output. Given that ViperGPT-style models successfully separate perception from reasoning, we seek to investigate whether the existing perception tools adequately recognize low-level primitives in vector graphics.

For VDLM, we explored two variants based on the choice of the reasoning module, with and without a Code Interpreter (CI). For the variant *without* a code interpreter, we leverage GPT-4<sup>‡§</sup> as our reasoner. For the variant *with* a code interpreter, given that the GPT-4 Chat Completion API does not natively support a code interpreter, we employ the GPT-4 Assistant API (Beta)<sup>¶</sup> for our experiments, designating the code interpreter as the sole tool available.

Since VDLM utilizes a pure text-based representation for reasoning, task instructions that assume visual inputs can become ambiguous. For example, in the task Angle Classification, it is unclear which angle the question is referring to if we are only given the coordinates of two undirected edges. Therefore, we design task-specific prompts that remove such ambiguity and are suitable for our PVD representation. Details about prompt design can be found in Appendix E.

**Results.** Table 1 displays the zero-shot accuracy for the evaluation tasks. We outline the key findings and insights as follows:

- (1) VDLM outperforms the state-of-the-art closed-source LMM, GPT-4V, by a large margin, highlighting the efficacy of our text-based disentangled framework in precise low-level perception and reasoning. We also observe that GPT-4 can make well-reasoned assumptions to creatively interpret the perception results or filter out unimportant information. For instance, as illustrated in Figure 2, it correctly infers the compositional object with two triangles as a “star”. See Figure 13 for the complete response.
- (2) Augmenting the reasoning model with code interpreters can be particularly helpful on tasks that require algorithmic reasoning. Examples include determining whether the positions of multiple objects fall within a specific range (in the NLVR task) and solving a complex maze using Depth-First Search (DFS) algorithm (in the 3×3 Maze Solving task).
- (3) The combination of ViperGPT and GPT-4 underperforms in these tasks, suggesting that existing vision-language models, such as GLIP and BLIP2, may have difficulty with

<sup>†</sup>GPT-4V model version: gpt-4-1106-vision-preview.

<sup>‡</sup><https://platform.openai.com/docs/guides/text-generation/chat-completions-api>

<sup>§</sup>GPT-4 model version: gpt-4-0125-preview.

<sup>¶</sup><https://platform.openai.com/docs/assistants/overview/agents>

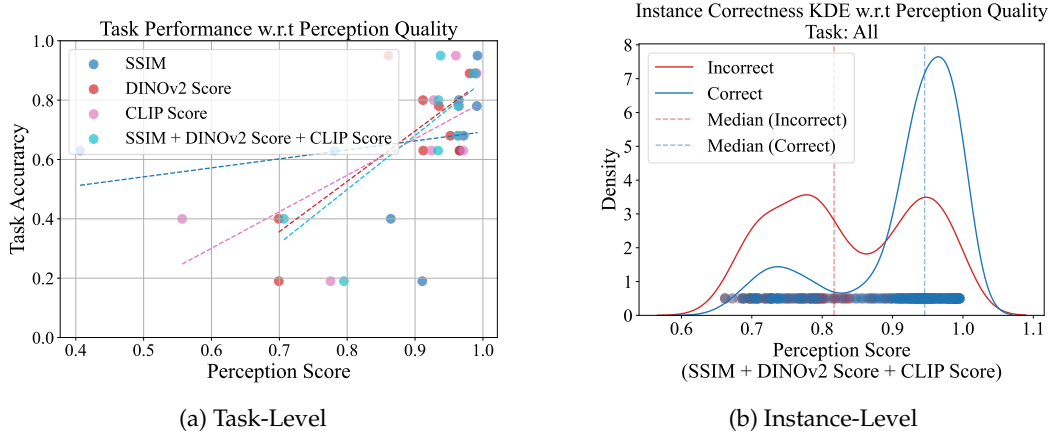


Figure 5: Correlation between perception quality and end-task performance. We observe a positive correlation between more precise perception and higher downstream accuracy.

low-level primitives such as angles and shapes. This is not surprising as they are trained on datasets that are heavily biased towards high-level, real-world objects, such as people and household items.

(4) On the Geoclidean task, VDLM achieves only comparable performance with GPT-4V. This suggests that certain visual attributes might be more effectively represented through image-based rather than symbolic representation. Further details are presented in §4.2.

## 4 Analysis

### 4.1 Perception Quality vs End-Task Performance

One advantage of a modular system is that enhancing an individual module can potentially improve the overall system. In this section, we explore whether a positive correlation exists between the quality of perception and end-task performance. To investigate this, we first define metrics to reflect the quality of the Primal Visual Description (PVD) perception. Upon generating a PVD perception result, we render it back into a raster image using our procedural image generator. We then compute a similarity score between the reconstructed image and the original input image as a measure of the perception performance. For measuring the similarity, we consider various approaches, including both pixel-based and embedding-based metrics. We adopt the Structural Similarity (SSIM) Index (Wang et al., 2004) score to assess pixel-level similarity. Additionally, to account for semantic similarity, we adopt a CLIP-score (Radford et al., 2021) and a DINOv2-score (Oquab et al., 2023), which are calculated as the cosine similarity of the flattened CLIP and DINOv2 embeddings, respectively.

In Figure 5, we visualize the impact of the perception quality on the downstream task performance at both the task and instance levels. In Figure 5a, each point denotes the accuracy of a task, with different colors representing different similarity metrics. The dashed lines depict linear regression results of the points, revealing a consistent positive correlation between perception quality and task accuracy across the metrics. Since the task-level accuracy may not be directly comparable across different tasks, we additionally perform an instance-level analysis using Kernel Density Estimation (KDE) on the correctness of all task instances with respect to their perception scores. As shown in Figure 5b, the “correct” distribution visibly skews to the area of higher perception scores, indicating that better perception tends to result in a correct final answer among all the tasks we evaluated. This finding is promising, suggesting that enhancing the perception module, even with a fixed reasoning model, can effectively boost downstream task performance.

## 4.2 Deep Dive into Failure Modes: A Transparent Error Analysis

The improved interpretability, resulting from Primal Visual Description’s disentangled perception and reasoning, allows us to conduct an in-depth analysis of the failure modes of VDLM. We find that both the SVG-to-PVD perception step and the LLM reasoning step can contribute to incorrect final answers. On tasks that demand more complex reasoning, such as NLVR and Maze Solving, reasoning errors become more prevalent; otherwise, perception errors most directly contribute to poor performance. We identify several prevalent error types for both perception and reasoning.

**Common perception errors** include: failure to faithfully perceive novel shapes that cannot be covered by the Primal Visual Description (PVD); failure to capture accurate constraints between primitives, such as a line exactly segmenting a circle, due to the random nature of the data generation on the positioning of objects; failure to capture very small objects, due to the heuristic thresholding in the incremental SVG decomposition algorithm.

**Common reasoning errors** include: failure to discover intentional constraints without being explicitly asked, such as automatically identifying that a rhombus is not the same concept as a general quadrilateral; failure in handling ambiguous instructions; failure in complex multi-step reasoning tasks, such as solving mazes.

We provide details and illustrative examples of these errors in Appendix B, along with a distribution of perception and reasoning errors from human analyses.

## 5 Related Work

**Visual shortcomings in large multimodal models (LMMs).** While state-of-the-art LMMs achieve strong performance on existing multimodal benchmarks (Goyal et al., 2017; Fu et al., 2023; Liu et al., 2023b;d; Yu et al., 2023; Li et al., 2023a), which primarily focus on natural images, recent work (Lu et al., 2023; Yue et al., 2023; Huang et al., 2023; Zhou et al., 2023; Hsu et al., 2022; Gao et al., 2023) has shown that they struggle with charts, geometric diagrams, and abstract scenes. This observation aligns with recent studies investigating visual shortcomings in LMMs. Tong et al. (2024) suggests that current LMMs struggle with visual details because the image-text contrastive pretraining of the CLIP visual backbone does not encourage the preservation of fine-grained visual features, such as orientation and quantity. To address this issue, recent studies have either leveraged the mixture-of-experts approach (Tong et al., 2024; Fan et al., 2024; Lu et al., 2024; Jain et al., 2023b), incorporating various types of vision encoders, such as SAM (Kirillov et al., 2023), DINOv2 (Oquab et al., 2023), or introduced auxiliary losses that emphasize local details during multimodal pretraining McKinzie et al. (2024); Bica et al. (2024); Varma et al. (2023). In this work, we propose a novel perspective for addressing this visual deficiency in vector graphics with text-based representations.

**Image Vectorization and Program Synthesis.** Generating vectorized or symbolic representations of visual inputs has been a topic of interest in both the NLP and computer vision communities. Recent work (Jain et al., 2023a; Ma et al., 2022; Vinker et al., 2022; Lee et al., 2023) has investigated generating SVG code or strokes from raster images. These methods typically rely on learning-based models and iterative optimizations, which can potentially introduce domain-specific biases and have slow inference. In this work, the end goal is not vectorizing images but interpreting and reasoning about visual concepts. Although Bubeck et al. (2023); Cai et al. (2023) have shown initial promise in using LLMs for directly understanding SVG code, as shown in § A.3, it is still quite limited. Therefore, we propose the intermediate Primal Visual Description and leverage a non-learning-based parsing algorithm (VTracer) for initial perception from images, which is appropriate for constructing large-scale (SVG, PVD) datasets. This work is also heavily inspired by related work in neural-symbolic models (Ritchie et al., 2016; Wu et al., 2017; Yi et al., 2018; Mao et al., 2019; Hsu et al., 2023; Zhang et al., 2023; Trinh et al., 2024). This paradigm aims to de-render visual scenes into structured representations, retrieve programs from input text, and execute these programs on the image representations. Instead of defining task-specific symbolic

programs, we extend the idea to learning a task-agnostic visual description that can be directly reasoned about by off-the-shelf large language models for task generalization.

**Disentangling Perception and Reasoning in LMMs.** Another closely related line of work has investigated disentangling visual processing and reasoning with visual programming (Gupta & Kembhavi, 2023; Surís et al., 2023; Ge et al., 2023; Wu & Xie, 2023) and tool-using (Wu et al., 2023; Liu et al., 2023c). These models leverage the code generation capabilities of LLMs to compose and employ a set of vision-language or vision-only models, such as object detection and image caption models, as subroutines for solving visual reasoning tasks. Despite promising performance on natural images, as shown in § 3, we find that these models are still limited by the existing vision-language models’ inability to process low-level primitives effectively.

## 6 Conclusions and Future Work

This work presents VDLM, a novel approach designed to address the limitations of Large Multimodal Models in performing precise low-level perception and reasoning tasks in vector graphics. By leveraging SVG representations and introducing an intermediate symbolic abstraction, VDLM enables precise capture of low-level visual features as well as direct harnessing of large language models for generalization. VDLM not only outperforms existing state-of-the-art LLMs such as GPT-4V but also enhances interpretability through its disentangled perception and reasoning process. The limitations of this work primarily stem from the representational capability of SVGs, which are mainly suited for effectively handling 2D vector graphics. Future directions include building a more general intermediate representation that can be extended from 2D vector graphics to 3D and natural images, and integrating the symbolic representation with the image representation to preserve important visual inductive biases.

## References

Rohan Anil, Sebastian Borgeaud, Yonghui Wu, Jean-Baptiste Alayrac, Jiahui Yu, Radu Soricut, Johan Schalkwyk, Andrew M. Dai, Anja Hauth, Katie Millican, David Silver, Slav Petrov, Melvin Johnson, Ioannis Antonoglou, Julian Schrittwieser, Amelia Glaese, Jilin Chen, Emily Pitler, Timothy P. Lillicrap, Angeliki Lazaridou, Orhan Firat, James Molloy, Michael Isard, Paul Ronald Barham, Tom Hennigan, Benjamin Lee, Fabio Viola, Malcolm Reynolds, Yuanzhong Xu, Ryan Doherty, Eli Collins, Clemens Meyer, Eliza Rutherford, Erica Moreira, Kareem Ayoub, Megha Goel, George Tucker, Enrique Piqueras, Maxim Krikun, Iain Barr, Nikolay Savinov, Ivo Danihelka, Becca Roelofs, Anaïs White, Anders Andreassen, Tamara von Glehn, Lakshman Yagati, Mehran Kazemi, Lucas Gonzalez, Misha Khalmi, Jakub Sygnowski, and et al. Gemini: A Family of Highly Capable Multimodal Models. *arXiv preprint arXiv:2312.11805*, 2023. URL <https://doi.org/10.48550/arXiv.2312.11805>.

Jinze Bai, Shuai Bai, Shusheng Yang, Shijie Wang, Sinan Tan, Peng Wang, Junyang Lin, Chang Zhou, and Jingren Zhou. Qwen-VL: A Frontier Large Vision-Language Model with Versatile Abilities. *arXiv preprint arXiv:2308.12966*, 2023. URL <https://doi.org/10.48550/arXiv.2308.12966>.

Ioana Bica, Anastasija Ilic, Matthias Bauer, Goker Erdogan, Matko Bosnjak, Christos Kaplantis, Alexey A. Gritsenko, Matthias Minderer, Charles Blundell, Razvan Pascanu, and Jovana Mitrovic. Improving Fine-Grained Understanding in Image-Text Pre-Training. *arXiv preprint arXiv:2401.09865*, 2024. URL <https://doi.org/10.48550/arXiv.2401.09865>.

Sébastien Bubeck, Varun Chandrasekaran, Ronen Eldan, Johannes Gehrke, Eric Horvitz, Ece Kamar, Peter Lee, Yin Tat Lee, Yuanzhi Li, Scott M. Lundberg, Harsha Nori, Hamid Palangi, Marco Túlio Ribeiro, and Yi Zhang. Sparks of Artificial General Intelligence: Early Experiments with GPT-4. *arXiv preprint arXiv:2303.12712*, 2023. URL <https://doi.org/10.48550/arXiv.2303.12712>.

Mu Cai, Zeyi Huang, Yuheng Li, Haohan Wang, and Yong Jae Lee. Leveraging Large Language Models for Scalable Vector Graphics-Driven Image Understanding. *arXiv preprint arXiv:2306.06094*, 2023. URL <https://doi.org/10.48550/arXiv.2306.06094>.

Alejandro Hernández Cano, Matteo Pagliardini, Andreas Köpf, Kyle Matoba, Amirkeivan Mohtashami, Xingyao Wang, Olivia Simin Fan, Axel Marmet, Deniz Bayazit, Igor Krawczuk, Zeming Chen, Francesco Salvi, Antoine Bosselut, and Martin Jaggi. EpfLLM Megatron-LLM, 2023. URL <https://github.com/epfLLM/Megatron-LLM>.

Lin Chen, Jinsong Li, Xiaoyi Dong, Pan Zhang, Conghui He, Jiaqi Wang, Feng Zhao, and Dahu Lin. ShareGPT4V: Improving Large Multi-Modal Models with Better Captions, 2023a. URL <https://doi.org/10.48550/arXiv.2311.12793>.

Zhe Chen, Jiannan Wu, Wenhui Wang, Weijie Su, Guo Chen, Sen Xing, Muyan Zhong, Qinglong Zhang, Xizhou Zhu, Lewei Lu, Bin Li, Ping Luo, Tong Lu, Yu Qiao, and Jifeng Dai. InternVL: Scaling up Vision Foundation Models and Aligning for Generic Visual-Linguistic Tasks. *arXiv preprint arXiv:2312.14238*, 2023b. URL <https://doi.org/10.48550/arXiv.2312.14238>.

Wei-Lin Chiang, Zhuohan Li, Zi Lin, Ying Sheng, Zhanghao Wu, Hao Zhang, Lianmin Zheng, Siyuan Zhuang, Yonghao Zhuang, Joseph E. Gonzalez, Ion Stoica, and Eric P. Xing. Vicuna: An Open-Source Chatbot Impressing GPT-4 with 90%\* ChatGPT Quality, March 2023. URL <https://1msys.org/blog/2023-03-30-vicuna/>.

Wenliang Dai, Junnan Li, Dongxu Li, Anthony Meng Huat Tiong, Junqi Zhao, Weisheng Wang, Boyang Li, Pascale Fung, and Steven C. H. Hoi. InstructBLIP: Towards General-purpose Vision-Language Models with Instruction Tuning. In *Advances in Neural Information Processing Systems 36: Annual Conference on Neural Information Processing Systems 2023 (NeurIPS)*, 2023. URL [http://papers.nips.cc/paper\\_files/paper/2023/hash/9a6a435e75419a836fe47ab6793623e6-Abstract-Conference.html](http://papers.nips.cc/paper_files/paper/2023/hash/9a6a435e75419a836fe47ab6793623e6-Abstract-Conference.html).

Xiaoran Fan, Tao Ji, Changhao Jiang, Shuo Li, Senjie Jin, Sirui Song, Junke Wang, Boyang Hong, Lu Chen, Guodong Zheng, Ming Zhang, Caishuang Huang, Rui Zheng, Zhiheng Xi, Yuhao Zhou, Shihan Dou, Junjie Ye, Hang Yan, Tao Gui, Qi Zhang, Xipeng Qiu, Xuanjing Huang, Zuxuan Wu, and Yu-Gang Jiang. MouSi: Poly-Visual-Expert Vision-Language Models. *arXiv preprint arXiv:2401.17221*, 2024. URL <https://doi.org/10.48550/arXiv.2401.17221>.

Chaoyou Fu, Peixian Chen, Yunhang Shen, Yulei Qin, Mengdan Zhang, Xu Lin, Zhenyu Qiu, Wei Lin, Jinrui Yang, Xiawu Zheng, Ke Li, Xing Sun, and Rongrong Ji. MME: A Comprehensive Evaluation Benchmark for Multimodal Large Language Models. *arXiv preprint arXiv:2306.13394*, 2023. URL <https://doi.org/10.48550/arXiv.2306.13394>.

Jiahui Gao, Renjie Pi, Jipeng Zhang, Jiacheng Ye, Wanjun Zhong, Yufei Wang, Lanqing Hong, Jianhua Han, Hang Xu, Zhenguo Li, and Lingpeng Kong. G-LLaVA: Solving Geometric Problem with Multi-Modal Large Language Model. *arXiv preprint arXiv:2312.11370*, 2023. URL <https://doi.org/10.48550/arXiv.2312.11370>.

Jiaxin Ge, Sanjay Subramanian, Baifeng Shi, Roei Herzig, and Trevor Darrell. Recursive Visual Programming. *arXiv preprint arXiv:2312.02249*, 2023. URL <https://doi.org/10.48550/arXiv.2312.02249>.

Yash Goyal, Tejas Khot, Douglas Summers-Stay, Dhruv Batra, and Devi Parikh. Making the V in VQA Matter: Elevating the Role of Image Understanding in Visual Question Answering. In *2017 IEEE Conference on Computer Vision and Pattern Recognition (CVPR)*, 2017. URL <https://doi.org/10.1109/CVPR.2017.670>.

Tianrui Guan, Fuxiao Liu, Xiyang Wu, Ruiqi Xian, Zongxia Li, Xiaoyu Liu, Xijun Wang, Lichang Chen, Furong Huang, Yaser Yacoob, et al. HallusionBench: An Advanced Diagnostic Suite for Entangled Language Hallucination and Visual Illusion in Large Vision-Language Models. In *IEEE/CVF Conference on Computer Vision and Pattern Recognition (CVPR)*, 2024. URL <https://arxiv.org/abs/2310.14566>.

Tanmay Gupta and Aniruddha Kembhavi. Visual Programming: Compositional Visual Reasoning without Training. In *IEEE/CVF Conference on Computer Vision and Pattern Recognition (CVPR)*, 2023. URL <https://doi.org/10.1109/CVPR52729.2023.01436>.

Joy Hsu, Jiajun Wu, and Noah D. Goodman. Geoclideo: Few-Shot Generalization in Euclidean Geometry. In *Advances in Neural Information Processing Systems 35: Annual Conference on Neural Information Processing Systems 2022 (NeurIPS)*, 2022. URL [http://papers.nips.cc/paper\\_files/paper/2022/hash/feb34ce77fc8b94c85d12e608b23ce67-Abstract-Datasets\\_and\\_Benchmarks.html](http://papers.nips.cc/paper_files/paper/2022/hash/feb34ce77fc8b94c85d12e608b23ce67-Abstract-Datasets_and_Benchmarks.html).

Joy Hsu, Jiayuan Mao, Joshua B. Tenenbaum, and Jiajun Wu. What's Left? Concept Grounding with Logic-Enhanced Foundation Models. In *Advances in Neural Information Processing Systems 36: Annual Conference on Neural Information Processing Systems 2023 (NeurIPS)*, 2023. URL [http://papers.nips.cc/paper\\_files/paper/2023/hash/79fea214543ba263952ac3f4e5452b14-Abstract-Conference.html](http://papers.nips.cc/paper_files/paper/2023/hash/79fea214543ba263952ac3f4e5452b14-Abstract-Conference.html).

Edward J. Hu, Yelong Shen, Phillip Wallis, Zeyuan Allen-Zhu, Yuanzhi Li, Shean Wang, Lu Wang, and Weizhu Chen. LoRA: Low-Rank Adaptation of Large Language Models. In *The Tenth International Conference on Learning Representations (ICLR)*, 2022. URL <https://openreview.net/forum?id=nZeVKeeFYf9>.

Kung-Hsiang Huang, Mingyang Zhou, Hou Pong Chan, Yi R. Fung, Zhenhailong Wang, Lingyu Zhang, Shih-Fu Chang, and Heng Ji. Do LVLMs Understand Charts? Analyzing and Correcting Factual Errors in Chart Captioning. *arXiv preprint arXiv:2312.10160*, 2023. URL <https://doi.org/10.48550/arXiv.2312.10160>.

Ajay Jain, Amber Xie, and Pieter Abbeel. VectorFusion: Text-to-SVG by Abstracting Pixel-Based Diffusion Models. In *IEEE/CVF Conference on Computer Vision and Pattern Recognition (CVPR)*, 2023a. URL <https://doi.org/10.1109/CVPR52729.2023.00190>.

Jitesh Jain, Jianwei Yang, and Humphrey Shi. VCoder: Versatile Vision Encoders for Multimodal Large Language Models. *arXiv preprint arXiv:2312.14233*, 2023b. URL <https://doi.org/10.48550/arXiv.2312.14233>.

Albert Q. Jiang, Alexandre Sablayrolles, Arthur Mensch, Chris Bamford, Devendra Singh Chaplot, Diego de Las Casas, Florian Bressand, Gianna Lengyel, Guillaume Lample, Lucile Saulnier, Lélio Renard Lavaud, Marie-Anne Lachaux, Pierre Stock, Teven Le Scao, Thibaut Lavril, Thomas Wang, Timothée Lacroix, and William El Sayed. Mistral 7B. *arXiv preprint arXiv:2310.06825*, 2023. URL <https://doi.org/10.48550/arXiv.2310.06825>.

Alexander Kirillov, Eric Mintun, Nikhila Ravi, Hanzi Mao, Chloé Rolland, Laura Gustafson, Tete Xiao, Spencer Whitehead, Alexander C. Berg, Wan-Yen Lo, Piotr Dollár, and Ross B. Girshick. Segment Anything. In *IEEE/CVF International Conference on Computer Vision (ICCV)*, 2023. URL <https://doi.org/10.1109/ICCV51070.2023.00371>.

Ranjay Krishna, Yuke Zhu, Oliver Groth, Justin Johnson, Kenji Hata, Joshua Kravitz, Stephanie Chen, Yannis Kalantidis, Li-Jia Li, David A. Shamma, Michael S. Bernstein, and Li Fei-Fei. Visual Genome: Connecting Language and Vision Using Crowd-sourced Dense Image Annotations. *Int. J. Comput. Vis.*, 123(1):32–73, 2017. URL <https://doi.org/10.1007/s11263-016-0981-7>.

Benno Krojer, Vaibhav Adlakha, Vibhav Vineet, Yash Goyal, Edoardo Maria Ponti, and Siva Reddy. Image Retrieval from Contextual Descriptions. In *Proceedings of the 60th Annual Meeting of the Association for Computational Linguistics (ACL)*, 2022. URL <https://doi.org/10.18653/v1/2022.acl-long.241>.

Joseph B Kruskal. On the Shortest Spanning Subtree of a Graph and the Traveling Salesman Problem. *Proceedings of the American Mathematical society*, 7(1):48–50, 1956.

Alexander Kuhnle and Ann A. Copestake. ShapeWorld - A New Test Methodology for Multimodal Language Understanding. *arXiv preprint arXiv:1704.04517*, 2017. URL <http://arxiv.org/abs/1704.04517>.

Hyundo Lee, Inwoo Hwang, Hyunsung Go, Won-Seok Choi, Kibeom Kim, and Byoung-Tak Zhang. Learning Geometry-Aware Representations by Sketching. In *IEEE/CVF Conference on Computer Vision and Pattern Recognition (CVPR)*, 2023. URL <https://doi.org/10.1109/CVPR52729.2023.02233>.

Bohao Li, Rui Wang, Guangzhi Wang, Yuying Ge, Yixiao Ge, and Ying Shan. SEED-Bench: Benchmarking Multimodal LLMs with Generative Comprehension. *arXiv preprint arXiv:2307.16125*, 2023a. URL <https://doi.org/10.48550/arXiv.2307.16125>.

Junnan Li, Dongxu Li, Silvio Savarese, and Steven C. H. Hoi. BLIP-2: Bootstrapping Language-Image Pre-training with Frozen Image Encoders and Large Language Models. In *International Conference on Machine Learning (ICML)*, 2023b. URL <https://proceedings.mlr.press/v202/li23q.html>.

Liunian Harold Li, Pengchuan Zhang, Haotian Zhang, Jianwei Yang, Chunyuan Li, Yiwu Zhong, Lijuan Wang, Lu Yuan, Lei Zhang, Jenq-Neng Hwang, Kai-Wei Chang, and Jianfeng Gao. Grounded Language-Image Pre-training. In *IEEE/CVF Conference on Computer Vision and Pattern Recognition (CVPR)*, 2022. URL <https://doi.org/10.1109/CVPR52688.2022.01069>.

Tsung-Yi Lin, Michael Maire, Serge J. Belongie, James Hays, Pietro Perona, Deva Ramanan, Piotr Dollár, and C. Lawrence Zitnick. Microsoft COCO: Common Objects in Context. In *Computer Vision - ECCV 2014 - 13th European Conference*, 2014. URL [https://doi.org/10.1007/978-3-319-10602-1\\_48](https://doi.org/10.1007/978-3-319-10602-1_48).

Haotian Liu, Chunyuan Li, Yuheng Li, and Yong Jae Lee. Improved Baselines with Visual Instruction Tuning. *arXiv preprint arXiv:2310.03744*, 2023a. URL <https://doi.org/10.48550/arXiv.2310.03744>.

Haotian Liu, Chunyuan Li, Qingyang Wu, and Yong Jae Lee. Visual Instruction Tuning. In *Advances in Neural Information Processing Systems 36: Annual Conference on Neural Information Processing Systems 2023 (NeurIPS), 2023b*. URL [http://papers.nips.cc/paper\\_files/paper/2023/hash/6dcf277ea32ce3288914faf369fe6de0-Abstract-Conference.html](http://papers.nips.cc/paper_files/paper/2023/hash/6dcf277ea32ce3288914faf369fe6de0-Abstract-Conference.html).

Shilong Liu, Hao Cheng, Haotian Liu, Hao Zhang, Feng Li, Tianhe Ren, Xueyan Zou, Jianwei Yang, Hang Su, Jun Zhu, Lei Zhang, Jianfeng Gao, and Chunyuan Li. LLaVA-Plus: Learning to Use Tools for Creating Multimodal Agents. *arXiv preprint arXiv:2311.05437*, 2023c. URL <https://doi.org/10.48550/arXiv.2311.05437>.

Yuan Liu, Haodong Duan, Yuanhan Zhang, Bo Li, Songyang Zhang, Wangbo Zhao, Yike Yuan, Jiaqi Wang, Conghui He, Ziwei Liu, Kai Chen, and Dahua Lin. MMBench: Is Your Multi-modal Model an All-around Player? *arXiv preprint arXiv:2307.06281*, 2023d. URL <https://doi.org/10.48550/arXiv.2307.06281>.

Haoyu Lu, Wen Liu, Bo Zhang, Bingxuan Wang, Kai Dong, Bo Liu, Jingxiang Sun, Tongzheng Ren, Zhuoshu Li, Hao Yang, Yaofeng Sun, Chengqi Deng, Hanwei Xu, Zhenda Xie, and Chong Ruan. DeepSeek-VL: Towards Real-World Vision-Language Understanding. *arXiv preprint arXiv:2403.05525*, 2024. URL <https://doi.org/10.48550/arXiv.2403.05525>.

Pan Lu, Hritik Bansal, Tony Xia, Jiacheng Liu, Chunyuan Li, Hannaneh Hajishirzi, Hao Cheng, Kai-Wei Chang, Michel Galley, and Jianfeng Gao. MathVista: Evaluating Math Reasoning in Visual Contexts with GPT-4V, Bard, and Other Large Multimodal Models. *arXiv preprint arXiv:2310.02255*, 2023. URL <https://doi.org/10.48550/arXiv.2310.02255>.

Xu Ma, Yuqian Zhou, Xingqian Xu, Bin Sun, Valerii Filev, Nikita Orlov, Yun Fu, and Humphrey Shi. Towards Layer-wise Image Vectorization. In *IEEE/CVF Conference on Computer Vision and Pattern Recognition (CVPR)*, 2022. URL <https://doi.org/10.1109/CVPR52688.2022.01583>.

Jiayuan Mao, Chuang Gan, Pushmeet Kohli, Joshua B. Tenenbaum, and Jiajun Wu. The Neuro-Symbolic Concept Learner: Interpreting Scenes, Words, and Sentences From Natural Supervision. In *7th International Conference on Learning Representations (ICLR)*, 2019. URL <https://openreview.net/forum?id=rJgMlhRctm>.

Kenneth Marino, Mohammad Rastegari, Ali Farhadi, and Roozbeh Mottaghi. OK-VQA: A Visual Question Answering Benchmark Requiring External Knowledge. In *IEEE Conference on Computer Vision and Pattern Recognition (CVPR)*, 2019. URL [http://openaccess.thecvf.com/content\\_CVPR\\_2019/html/Marino\\_OK-VQA\\_A\\_Visual\\_Question\\_Answering\\_Benchmark\\_Requiring\\_External\\_Knowledge\\_CVPR\\_2019\\_paper.html](http://openaccess.thecvf.com/content_CVPR_2019/html/Marino_OK-VQA_A_Visual_Question_Answering_Benchmark_Requiring_External_Knowledge_CVPR_2019_paper.html).

Brandon McKinzie, Zhe Gan, Jean-Philippe Fauconnier, Sam Dodge, Bowen Zhang, Philipp Dufter, Dhruti Shah, Xianzhi Du, Futang Peng, Floris Weers, Anton Belyi, Haotian Zhang, Karanjeet Singh, Doug Kang, Ankur Jain, Hongyu Hè, Max Schwarzer, Tom Gunter, Xiang Kong, Aonan Zhang, Jianyu Wang, Chong Wang, Nan Du, Tao Lei, Sam Wiseman, Guoli Yin, Mark Lee, Zirui Wang, Ruoming Pang, Peter Grasch, Alexander Toshev, and Yinfei Yang. MM1: Methods, Analysis & Insights from Multimodal LLM Pre-training. *arXiv preprint arXiv:2403.09611*, 2024. URL <https://doi.org/10.48550/arXiv.2403.09611>.

OpenAI. GPT-4 Technical Report, 2023a.

OpenAI. GPT-4V(ision) System Card, 2023b. URL [https://cdn.openai.com/papers/GPTV\\_System\\_Card.pdf](https://cdn.openai.com/papers/GPTV_System_Card.pdf).

Maxime Oquab, Timothée Darcet, Théo Moutakanni, Huy Vo, Marc Szafraniec, Vasil Khaldov, Pierre Fernandez, Daniel Haziza, Francisco Massa, Alaaeldin El-Nouby, Mahmoud Assran, Nicolas Ballas, Wojciech Galuba, Russell Howes, Po-Yao Huang, Shang-Wen Li, Ishan Misra, Michael G. Rabbat, Vasu Sharma, Gabriel Synnaeve, Hu Xu, Hervé Jégou,

Julien Mairal, Patrick Labatut, Armand Joulin, and Piotr Bojanowski. DINOv2: Learning Robust Visual Features without Supervision. *arXiv preprint arXiv:2304.07193*, 2023. URL <https://doi.org/10.48550/arXiv.2304.07193>.

Alec Radford, Jong Wook Kim, Chris Hallacy, Aditya Ramesh, Gabriel Goh, Sandhini Agarwal, Girish Sastry, Amanda Askell, Pamela Mishkin, Jack Clark, Gretchen Krueger, and Ilya Sutskever. Learning Transferable Visual Models From Natural Language Supervision. In *Proceedings of the 38th International Conference on Machine Learning (ICML)*, 2021. URL <http://proceedings.mlr.press/v139/radford21a.html>.

Daniel Ritchie, Anna Thomas, Pat Hanrahan, and Noah D. Goodman. Neurally-Guided Procedural Models: Amortized Inference for Procedural Graphics Programs using Neural Networks. In *Advances in Neural Information Processing Systems 29: Annual Conference on Neural Information Processing Systems 2016 (NeurIPS)*, 2016. URL <https://proceedings.neurips.cc/paper/2016/hash/40008b9a5380fcacce3976bf7c08af5b-Abstract.html>.

Dustin Schwenk, Apoorv Khandelwal, Christopher Clark, Kenneth Marino, and Roozbeh Mottaghi. A-OKVQA: A Benchmark for Visual Question Answering Using World Knowledge. In *Computer Vision - ECCV 2022 - 17th European Conference*, 2022. URL [https://doi.org/10.1007/978-3-031-20074-8\\_9](https://doi.org/10.1007/978-3-031-20074-8_9).

Oleksii Sidorov, Ronghang Hu, Marcus Rohrbach, and Amanpreet Singh. TextCaps: A Dataset for Image Captioning with Reading Comprehension. In *Computer Vision - ECCV 2020 - 16th European Conference*, 2020. URL [https://doi.org/10.1007/978-3-030-58536-5\\_44](https://doi.org/10.1007/978-3-030-58536-5_44).

Alane Suhr, Mike Lewis, James Yeh, and Yoav Artzi. A Corpus of Natural Language for Visual Reasoning. In *Proceedings of the 55th Annual Meeting of the Association for Computational Linguistics (ACL)*, 2017. URL <https://doi.org/10.18653/v1/P17-2034>.

Dídac Surís, Sachit Menon, and Carl Vondrick. ViperGPT: Visual Inference via Python Execution for Reasoning. In *IEEE/CVF International Conference on Computer Vision (ICCV)*, 2023. URL <https://doi.org/10.1109/ICCV51070.2023.01092>.

Shengbang Tong, Zhuang Liu, Yuexiang Zhai, Yi Ma, Yann LeCun, and Saining Xie. Eyes Wide Shut? Exploring the Visual Shortcomings of Multimodal LLMs. *arXiv preprint arXiv:2401.06209*, 2024. URL <https://doi.org/10.48550/arXiv.2401.06209>.

Trieu H. Trinh, Yuhuai Wu, Quoc V. Le, He He, and Thang Luong. Solving Olympiad Geometry without Human Demonstrations. *Nat.*, 625(7995):476–482, 2024. URL <https://doi.org/10.1038/s41586-023-06747-5>.

Maya Varma, Jean-Benoit Delbrouck, Sarah M. Hooper, Akshay Chaudhari, and Curtis P. Langlotz. ViLLA: Fine-Grained Vision-Language Representation Learning from Real-World Data. In *IEEE/CVF International Conference on Computer Vision (ICCV)*, 2023. URL <https://doi.org/10.1109/ICCV51070.2023.02031>.

Yael Vinker, Ehsan Pajouheshgar, Jessica Y. Bo, Roman Christian Bachmann, Amit Haim Bermano, Daniel Cohen-Or, Amir Zamir, and Ariel Shamir. CLIPasso: Semantically-aware Object Sketching. *ACM Trans. Graph.*, 41(4):86:1–86:11, 2022. URL <https://doi.org/10.1145/3528223.3530068>.

VTracer. Vtracer. URL <https://www.visioncortex.org/vtracer-docs>.

Xingyao Wang, Yangyi Chen, Lifan Yuan, Yizhe Zhang, Yunzhu Li, Hao Peng, and Heng Ji. Executable Code Actions Elicit Better LLM Agents. *arXiv preprint arXiv:2402.01030*, 2024. URL <https://doi.org/10.48550/arXiv.2402.01030>.

Zhou Wang, Alan C. Bovik, Hamid R. Sheikh, and Eero P. Simoncelli. Image Quality Assessment: From Error Visibility to Structural Similarity. *IEEE Trans. Image Proces.*, 13(4):600–612, 2004. URL <https://doi.org/10.1109/TIP.2003.819861>.

Chenfei Wu, Shengming Yin, Weizhen Qi, Xiaodong Wang, Zecheng Tang, and Nan Duan. Visual ChatGPT: Talking, Drawing and Editing with Visual Foundation Models. *arXiv preprint arXiv:2303.04671*, 2023. URL <https://doi.org/10.48550/arXiv.2303.04671>.

Jiajun Wu, Joshua B. Tenenbaum, and Pushmeet Kohli. Neural Scene De-rendering. In *2017 IEEE Conference on Computer Vision and Pattern Recognition (CVPR)*, 2017. URL <https://doi.org/10.1109/CVPR.2017.744>.

Penghao Wu and Saining Xie. V\*: Guided Visual Search as a Core Mechanism in Multimodal LLMs. *arXiv preprint arXiv:2312.14135*, 2023. URL <https://doi.org/10.48550/arXiv.2312.14135>.

Ke Yang, Jiateng Liu, John Wu, Chaoqi Yang, Yi R. Fung, Sha Li, Zixuan Huang, Xu Cao, Xingyao Wang, Yiquan Wang, Heng Ji, and Chengxiang Zhai. If LLM Is the Wizard, Then Code Is the Wand: A Survey on How Code Empowers Large Language Models to Serve as Intelligent Agents. *arXiv preprint arXiv:2401.00812*, 2024. URL <https://doi.org/10.48550/arXiv.2401.00812>.

Kexin Yi, Jiajun Wu, Chuang Gan, Antonio Torralba, Pushmeet Kohli, and Josh Tenenbaum. Neural-Symbolic VQA: Disentangling Reasoning from Vision and Language Understanding. In *Advances in Neural Information Processing Systems 31: Annual Conference on Neural Information Processing Systems 2018 (NeurIPS)*, 2018. URL <https://proceedings.neurips.cc/paper/2018/hash/5e388103a391daabe3de1d76a6739cccd-Abstract.html>.

Weihao Yu, Zhengyuan Yang, Linjie Li, Jianfeng Wang, Kevin Lin, Zicheng Liu, Xinchao Wang, and Lijuan Wang. MM-Vet: Evaluating Large Multimodal Models for Integrated Capabilities. *arXiv preprint arXiv:2308.02490*, 2023. URL <https://doi.org/10.48550/arXiv.2308.02490>.

Xiang Yue, Yuansheng Ni, Kai Zhang, Tianyu Zheng, Ruqi Liu, Ge Zhang, Samuel Stevens, Dongfu Jiang, Weiming Ren, Yuxuan Sun, Cong Wei, Botao Yu, Ruibin Yuan, Renliang Sun, Ming Yin, Boyuan Zheng, Zhenzhu Yang, Yibo Liu, Wenhao Huang, Huan Sun, Yu Su, and Wenhui Chen. MMMU: A Massive Multi-discipline Multimodal Understanding and Reasoning Benchmark for Expert AGI. *arXiv preprint arXiv:2311.16502*, 2023. URL <https://doi.org/10.48550/arXiv.2311.16502>.

Sharon Zhang, Jiaju Ma, Jiajun Wu, Daniel Ritchie, and Maneesh Agrawala. Editing Motion Graphics Video via Motion Vectorization and Transformation. *ACM Trans. Graph.*, 42(6):229:1–229:13, 2023. URL <https://doi.org/10.1145/3618316>.

Mingyang Zhou, Yi Ren Fung, Long Chen, Christopher Thomas, Heng Ji, and Shih-Fu Chang. Enhanced Chart Understanding via Visual Language Pre-training on Plot Table Pairs. In *Findings of the Association for Computational Linguistics: ACL 2023*, 2023. URL <https://doi.org/10.18653/v1/2023.findings-acl.85>.

## Supplementary Material for Text-Based Reasoning About Vector Graphics

The appendix is organized as follows: In Appendix A, we present preliminary experiments comparing SVG and image-based representations. In Appendix B, we include details on error analyses, and in Appendix C, we describe Primal Visual Description details. Appendix D shows the full input and output from GPT-4 for the maze-solving example depicted in Figure 2. Task prompts and newly constructed downstream task datasets can be found in Appendices E and F, respectively. In Appendix G, we include detailed statistics for all of the datasets we used.

### A Preliminary Experiments on SVG Representations

We introduce a suite of probing tasks to evaluate current LMMs’ capabilities in performing tasks with vector graphics. The results show that even state-of-the-art LMMs, such as GPT-4V, struggle with tasks that require precise perception of low-level primitives, such as comparing the lengths of two lines. We then investigate where this deficiency originates and propose an alternative representation, Scalable Vector Graphics (SVG), for representing such precise low-level features. We find that, compared to image-based representations, SVG representations can be more efficient for visual reasoning on vector graphics. However, they are not without their own limitations, which we will elaborate on in § A.3.

#### A.1 Image and SVG Representations

In the probing tasks, we include both discriminative and generative tasks, each with varying levels of emphasis on low-level visual details. Illustrations of the input and output examples are available in Figure 6. We additionally include a non-vector-graphics task, Clevr QA, which consists of realistic 3D rendered scenes. This is to test the limits of SVG representations in encoding 3D objects within realistic images. Detailed statistics of these tasks can be found in Table 4.

For each task, we consider two evaluation settings: zero-shot and fine-tuning. We explore two types of representations for the input image: (1) direct use of the image pixels, encoding them into patch embeddings with an image encoder, e.g., CLIP (Radford et al., 2021); (2) conversion of the image into SVG code using a rule-based raster-to-SVG converter (VTracer).

For fine-tuning with the image input, we instruction-finetune Llava-v1.5-7b (including the LLM-backbone and the projection layer) using Lora (Hu et al., 2022) on the training set for one epoch. For fine-tuning with the SVG input, we only fine-tune the LLM backbone of Llava-v1.5, Vicuna (Chiang et al., 2023), using Lora for one epoch, with the input image’s SVG code concatenated in the context. The results are shown in Table 2. Key observations include:

- (1) The SOTA open-source LMM, Llava-v1.5, struggles to achieve non-trivial performance on most probing tasks even with dedicated fine-tuning. On tasks with binary choices, Llava tends to predict homogeneous answers, disregarding differences in the input image.
- (2) The SOTA closed-source LMM, GPT-4V, excels on task Line or Angle, which focuses on querying the high-level semantics of the primitive concept (“what’s in the image”). However, its performance significantly decreases on tasks requiring more precise low-level perception, e.g., Angle Classification and Length Comparison.
- (3) Fine-tuning the LLM backbone, Vicuna, with SVG inputs consistently outperforms fine-tuning the entire Llava model with image inputs. This highlights the potential of using SVG as an alternative representation in vector graphics.
- (4) We note that SVG may inherently be inefficient in representing rendered 3D scenes and realistic images due to factors like camera perspectives, lighting, and shadows. While our focus in this work is on vector graphics, we leave the extension to other domains for future exploration.

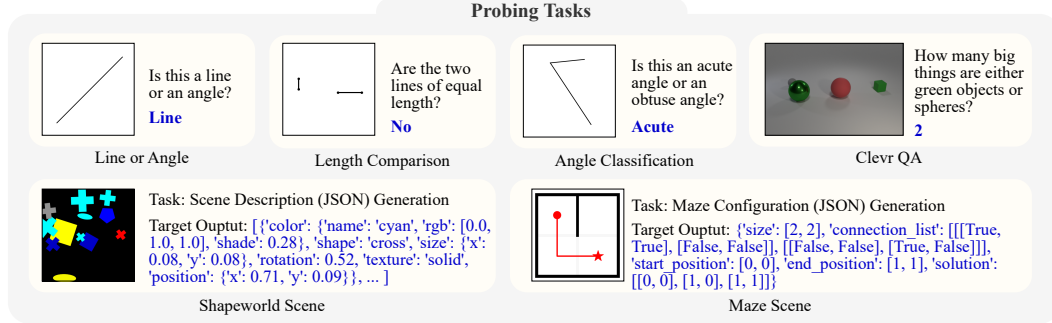


Figure 6: Illustration of the probing tasks. The four tasks at the top are question-answering tasks, while the two tasks at the bottom are scene-generation tasks. The goal of the scene-generation tasks is to generate the entire structured scene description following a predefined schema.

		Input Type	Line or Angle	Angle Classification	Length Comparison	Clevr QA
Zero-Shot	GPT-4V	Image	1.00	0.58	0.57	0.57
	GPT-4	SVG	0.45	0.47	0.60	0.36
Finetuned	Llava-v1.5-7b	Image	0.50	0.50	0.50	0.45
	Vicuna	SVG	0.93	0.70	0.99	0.54
		Input Type	Shapeworld Scene shape (acc↑) position (l2↓)	Maze Scene connectivity (acc↑) start-pos (acc↑) end-pos (acc↑)		
Zero-Shot	GPT-4V	Image	0.33	0.27	0.27	0.21
Finetuned	Llava-v1.5-7b	Image	0.04	0.67	0.26	0.03
	Vicuna	SVG	0.15	0.07	0.54	0.08

Table 2: Probing task results. We report the accuracy for the four question-answering tasks at the top. At the bottom, we use different metrics for different fields in the predicted scene description JSON. “acc” refers to accuracy (larger is better) while “l2” refers to the Euclidean distance between the predicted and ground truth [x, y] coordinates (lower is better). Scores with a blue background denote the better fine-tuned method compared to the SVG and Image representation. Scores with a red background denote tasks where fine-tuned methods cannot outperform zero-shot GPT-4V. Detailed analysis can be found in § A.1.

## A.2 Llava’s Failure Mode in Visual Reasoning with Vector Graphics

We further investigate whether the difficulty in understanding low-level visual features of Llava models stems from (1) the visual backbone itself, i.e., CLIP, or (2) the bridge between the visual backbone and the LLM backbone. We include a set of **Linear Probing** experiments on three binary classification probing tasks, where we train a simple linear classifier based on the visual backbone features (before and after projection) of the Llava model. As shown in Figure 7:

- (1) In tasks requiring more precise low-level perception, such as Angle Classification and Length Comparison, CLIP embeddings are inherently less effective at capturing relevant features. Furthermore, as shown in Figure 8, in some tasks, e.g., Length Comparison, linear regression even fails to achieve 90%+ training accuracy after 10 epochs of training, struggling to converge.
- (2) When connected to an LLM using the projection layer, the visual features in Llava become less effective for low-level visual reasoning. Additionally, there is a significant gap between linear probing and instruction fine-tuning performance. These results suggest that even if the backbone does preserve useful features, the LLM cannot effectively leverage those visual tokens after projection.

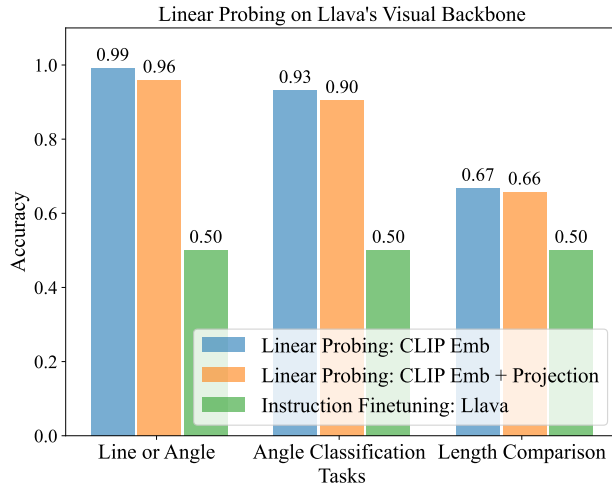


Figure 7: The average accuracy of linear probing, computed across ten epochs. Detailed training and testing scores for each epoch can be found in Figure 8. The results demonstrate that (1) CLIP embeddings are less effective for tasks requiring precise perception, such as Length Comparison, in comparison to tasks that emphasize on higher-level semantics, such as Line or Angle; (2) connecting to an LLM through the widely-used Llava-style architecture results in further diminished performance on tasks involving low-level visual details.

We hypothesize that the failure mode likely stems from the multimodal pretraining and instruction-tuning paradigm, where the tasks are biased towards high-level semantics, such as image captioning (Lin et al., 2014; Sidorov et al., 2020) and natural-image-based VQA (Goyal et al., 2017; Krishna et al., 2017; Marino et al., 2019; Schwenk et al., 2022). The training mixtures (Liu et al., 2023b;a; Dai et al., 2023; Chen et al., 2023a) for current LMMs predominantly focus on high-level features of images, providing little incentive for models to retain low-level visual details. For example, the caption of an image containing a 2D maze, such as the one shown in Figure 2, is likely to be “A  $2 \times 2$  maze with black lines, a red circle and a star.” and may not include detailed configurations of the mazes, such as the precise locations of the walls, the red circle, and the red star.

### A.3 Remaining Challenges of Using SVG Representations

Although we have demonstrated that SVG can serve as a promising alternative representation for reasoning about vector graphics, we identify several remaining challenges:

- (1) Pretrained LLMs, including the most capable ones such as GPT-4 (OpenAI, 2023a), possess limited out-of-the-box understanding of SVG code. This limitation is evidenced by the low zero-shot performance of GPT-4 with SVG input (see row 2 in Table 2).
- (2) Even after finetuning, the SVG-based LLM may still underperform zero-shot GPT-4V on certain tasks, particularly those involving complex scenes, such as Shapeworld Scene and Maze Scene. In these instances, the SVG code becomes excessively verbose. These findings suggest that learning a model to directly comprehend the raw SVG code of an entire image poses significant challenges.
- (3) A fundamental challenge, irrespective of the chosen representation for visual input, is the lack of generalization capability to unseen tasks and various vector graphics image domains. If we rely on existing LMM training mixtures, even any image can be converted into SVG code, the tasks remain biased towards high-level semantics. In addition, it is infeasible to directly manually construct and annotate  $\langle$ SVG, question, answer $\rangle$  pairs covering diverse tasks with vector graphics.

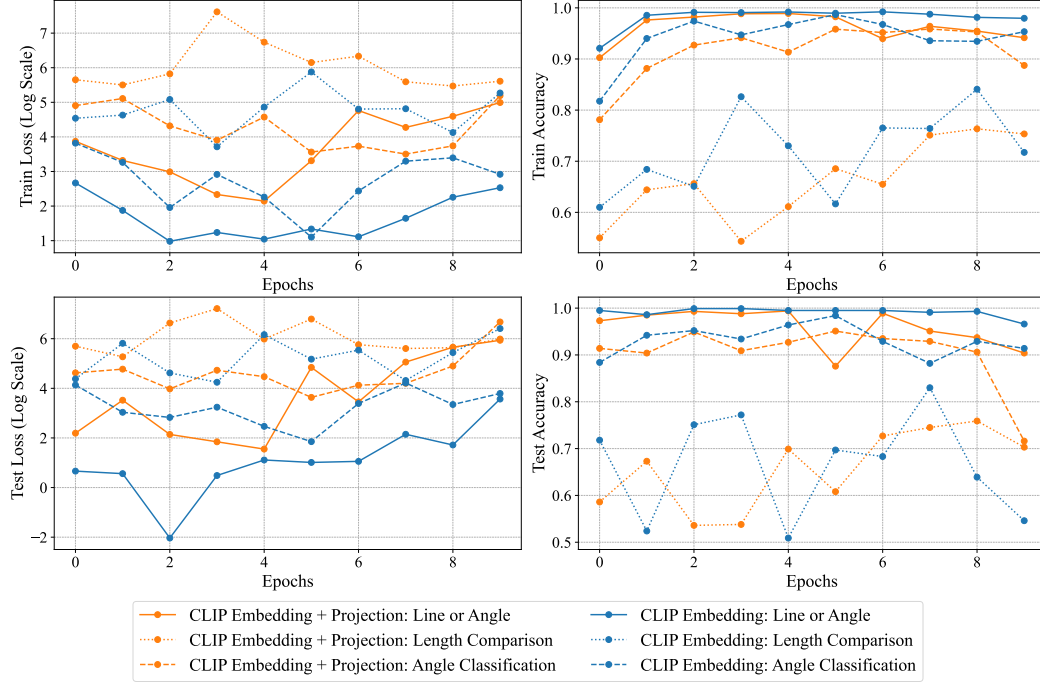


Figure 8: Linear probing training details: Different line styles represent different tasks, while different colors refer to different visual embeddings used for training the linear classifier. The training loss (top-left) shows that the projected embedding (orange lines) learns at a slower pace compared to the original CLIP embedding (blue lines). The training accuracy (top-right) reveals that for certain tasks, such as Length Comparison, the model continues to struggle with overfitting the training set even after 10 epochs.

These challenges motivated us to propose another layer of abstraction, the Primal Visual Description, aimed at bridging the gap between low-level perception and high-level language reasoning on downstream tasks.

## B Error Analysis Details

As introduced in § 2, the proposed VDLM consists of two stages focused on perception—namely, Image-to-SVG and SVG-to-PVD, and one stage focused on reasoning, i.e., PVD-to-final answer. We aim to investigate the errors in both the perception and reasoning modules.

For each task, we manually examine 10 error cases and determine whether the error primarily stems from the perception stage or the reasoning stage. We task a human with reviewing the reconstructed image from the Primal Visual Description representation and assessing the question of the task instance. If, for a human, the reconstructed image is still insufficient for solving the task, we classify this error as a perception error. Otherwise, it is categorized as a reasoning error. Figure 9 illustrates the distribution of errors between perception and reasoning stages. We further identify some typical categories of perception and reasoning errors as follows:

**Common perception errors.** (1) **Novel shapes not covered by the Primal Visual Description (PVD):** For example, as visualized in Figure 10, the Shapeworld dataset includes a “semicircle” shape type which is not in the PVD ontology; we see that the learned SVG-to-PVD model tends to predict it as an ellipse.

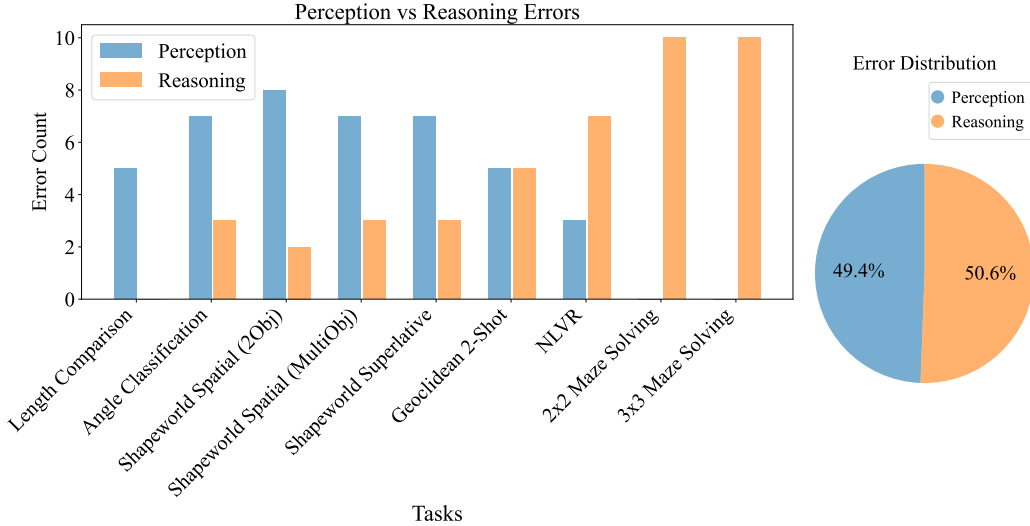


Figure 9: Error distribution between perception and reasoning.

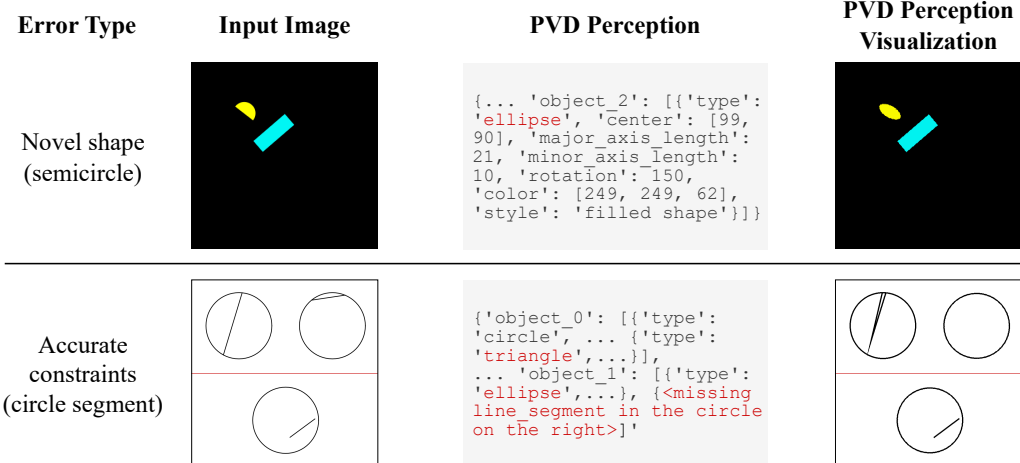


Figure 10: Perception error examples. The example at the top illustrates an error wherein the SVG-to-PVD model predicts a semicircle as an ellipse. The example at the bottom demonstrates that the SVG-to-PVD model struggles to decode overlapping primitives with accurate constraints, such as a segment of a circle.

(2) **Accurate constraints between primitives:** Although the PVD accommodates scenarios where multiple objects of the same color overlap, the attributes, e.g., position, of each object are decided independently and randomly. Thus, the SVG-to-PVD model often fails to capture intentional constraints between objects; for example, a line that perfectly segments a circle. These constraints are particularly emphasized in the Geoclidean 2-shot Learning task (Figure 10), where VDLM struggles to outperform GPT-4V.

(3) **Very small objects:** During inference, the iterative decomposition process heuristically ignores SVG paths that only contribute only minor differences to the reconstructed image. This method effectively reduces noise from the rule-based image-to-SVG converter but may omit very small objects in some cases. Adjusting this threshold is necessary for specific scenarios.

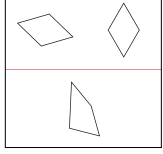
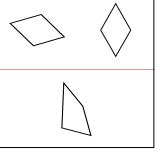
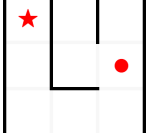
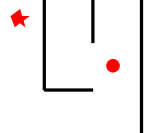
Error Type	Input Image	PVD Perception Visualization	Reasoning Model (GPT-4) Response
Discovering constraints (Rhombus v.s. Quadrilateral)			<p>To analyze the given JSON and identify the pattern and constraints of the reference and test concepts, let's break down the information provided for each object:</p> <ol style="list-style-type: none"> <li>**Object 0** (Test Example): <ul style="list-style-type: none"> <li>Type: Polygon</li> <li>Vertices: [(304, 416), (395, 527), (433, 665), (295, 629)]</li> <li>Characteristics: Outlined shape, black color, polygon with 4 vertices.</li> </ul> </li> <li>**Object 1** (Reference Example 1): <ul style="list-style-type: none"> <li>Type: Polygon ...</li> </ul> </li> <li>**Object 2** (Reference Example 2): <ul style="list-style-type: none"> <li>Type: Polygon ...</li> </ul> </li> </ol> <p>Given the descriptions, the reference examples (Object 1 and Object 2) and the test example (Object 0) are all polygons with 4 vertices, suggesting they are quadrilaterals...</p> <p>Given the information and assuming the concept involves quadrilaterals without requiring them to have uniform angles or sides (since we cannot precisely measure them from the given data), the test example appears to follow the same broad concept of being a quadrilateral as the reference examples.</p>
Algorithmic reasoning (Inferring maze connectivity)			<p>By examining the grid lines, we can determine where the walls are and thus infer the connections. However, the JSON doesn't directly specify the walls between cells, but we can deduce this from the absence of grid lines between cells.</p> <p>For simplicity, let's assume a fully connected grid without internal walls (as the JSON doesn't specify walls between cells explicitly), and then adjust based on typical maze patterns:</p> <ul style="list-style-type: none"> <li>**Vertical Connections:** All true, indicating no vertical walls between cells.</li> <li>**Horizontal Connections:** All true, indicating no horizontal walls between cells.</li> </ul> <p>... {"solution": "[[1, 1], [0, 0]]"}</p>

Figure 11: Reasoning error examples: The example at the top demonstrates that the reasoning model fails to uncover the deeper constraints within the perceived polygons. It is able to recognize that they are all quadrilaterals but unable to further discern that the reference concepts are rhombuses with four equal sides, while the test concept is not. The example at the bottom illustrates that the reasoning model struggles to infer connectivity based on the perceived grid, thus failing to provide the correct solution.

**Common reasoning errors.** (1) **Discovering intentional constraints:** Without specific queries, the reasoning model can fail to identify intentional constraints. For example, differentiating a rhombus from a general quadrilateral, as shown in Figure 11.

(2) **Handling ambiguity:** Visual inputs sometimes provide useful inductive biases that can help the model better understand the task or make reasonable assumptions when the instructions are ambiguous. For instance, when presenting an angle in an image and asking whether it is an acute or obtuse angle, as in Figure 4, it is visually straightforward to assume that the angle is defined by the middle point as the vertex with rays extending outwards. However, without such visual cues, reasoning over pure symbolic representations makes it challenging to infer which angle the question refers to among the detected undirected edges. To mitigate ambiguity, adding more precise instructions for VDLM is necessary in some tasks.

(3) **Algorithmic reasoning:** Language-based reasoners can struggle with complex multi-step reasoning tasks, such as inferring the connectivity (Figure 11) of a maze using the vertices and edges of the grid in pixel coordinates, or counting the number of objects located within a certain box.

## C Primal Visual Description (PVD) Details

**PVD JSON schema definition:** See Figure 12.

**Generation procedures (Single Object):**

- **Circle:** Randomly sample a center and a radius to draw a circle within the canvas.

Types	Schema	Example
Circle	<pre>{   "type": "circle",   "center": [x, y],   "radius": r,   "color": [r, g, b],   "style": "filled shape" or "outlined shape",   "line_width": d (if style is "outlined") }</pre>	<pre>{   "type": "circle",   "center": [205, 210],   "radius": 117,   "color": [193, 190, 165],   "style": "outlined shape",   "line_width": 9 }</pre>
Ellipse	<pre>{   "type": "ellipse",   "center": [x, y],   "major_axis_length": 11,   "minor_axis_length": 12,   "rotation": 0,   "color": [r, g, b],   "style": "filled shape" or "outlined shape",   "line_width": d (if style is "outlined") }</pre>	<pre>{   "type": "ellipse",   "center": [278, 166],   "major_axis_length": 147,   "minor_axis_length": 60,   "rotation": 16,   "color": [85, 220, 98],   "style": "filled shape" }</pre>
Rectangle	<pre>{   "type": "rectangle" or "triangle"   or "polygon",   "vertices": [[x1, y1], [x2, y2], ...]   "color": [r, g, b],   "style": "filled shape" or "outlined shape",   "line_width": d (if style is "outlined") }</pre>	
Triangle		<pre>{   "type": "triangle",   "vertices": [[452, 418], [298, 113],   [266, 255]],   "color": [165, 170, 141],   "style": "filled shape", }</pre>
Polygon		
Line Segment	<pre>{   "type": "line_segment",   "vertices": [[x1, y1], [x2, y2]]   "color": [r, g, b],   "line_width": d }</pre>	<pre>{   "type": "line segment",   "vertices": [[822, 114], [93, 20]],   "color": [166, 32, 97],   "line_width": 10 }</pre>
Grid	<pre>{   "type": "grid",   "vertices": [[x1, y1], [x2, y2], ...],   "edges": [[[x1, y1], [x2, y2]], ...],   "color": [r, g, b],   "line_width": d }</pre>	<pre>{   "type": "grid",   "vertices": [[73, 214], [73, 640],   [215, 214], [215, 640]],   "edges": [[[73, 214], [73, 640]],   [[215, 214], [215, 640]],   [[73, 640], [215, 640]]],   "color": [23, 31, 120],   "line_width": 3 }</pre>
Path	<pre>{   "type": "path",   "vertices": [[x1, y1], [x2, y2], ...],   "edges": [[[x1, y1], [x2, y2]], ...],   "color": [r, g, b],   "line_width": d }</pre>	<pre>{   "type": "path",   "vertices": [[59, 69], [17, 330],   [61, 77]],   "edges": [[[59, 69], [17, 330]],   [[17, 330], [61, 77]]],   "color": [98, 28, 0],   "line_width": 5 }</pre>
Graph	<pre>{   "type": "line drawing",   "vertices": [[x1, y1], [x2, y2], ...],   "edges": [[[x1, y1], [x2, y2]], ...],   "color": [r, g, b],   "line_width": d }</pre>	<pre>{   "type": "line drawing",   "vertices": [[399, 497], [433, 823],   [483, 570], [531, 443], [534, 578]],   "edges": [[[399, 497], [483, 570]],   [[531, 443], [534, 578]],   [[483, 570], [534, 578]],   [[483, 570], [433, 823]],   [[534, 578], [433, 823]]],   "color": [254, 230, 139],   "line_width": 9 }</pre>

Figure 12: PVD JSON schema definition.

- **Ellipse:** Randomly sample a center, a major axis, and a minor axis, then randomly rotate by an angle. Verify if the ellipse is largely within the canvas; if not, try again.
- **Rectangle:** Randomly sample a top-left corner, a width, and a height, then randomly rotate by an angle. Verify if the rectangle is largely within the canvas; if not, try again.
- **Triangle:** Randomly sample three points as vertices to draw a triangle. Check if the area is larger than a threshold; if not, try again.
- **Polygon:** Randomly sample  $N \in [5, 20]$  points. Order the points with respect to the centroid so that no intersections will happen when connected with a polyline. Draw a polygon with the sampled points. Check if the polygon has an area larger than a threshold; if not, try again.

	Style	Concept	# Instances
Single Object	Filled or Outlined	Circle	10K
		Ellipse	10K
		Rectangle	10K
		Triangle	10K
		Polygon	20K
	Outlined	Line Segment	10K
		Grid	10K
		Path	10K
		Graph	10K
Composition	Filled	Circle	5K
		Rectangle	5K
		Triangle	5K
		Line Segment	5K
	Outlined	Circle	10K
		Rectangle	10K
		Triangle	10K
		Line Segment	10K
<b>Total</b>			160K

Table 3: PVD 160K dataset statistics.

- **Path:** Randomly and iteratively sample  $N \in [3, 16]$  points, connect the newly sampled point with the previous point to form a line segment. Verify if the newly added line segment does not intersect with any of the previous line segments; if yes, resample the point.
- **Grid:** Sample a grid of points with a size  $M \times N$  where  $M, N \in [2, 6]$ . First, use Depth First Search (DFS) algorithm to connect all grid vertices into a connected graph. Then randomly add additional edges between adjacent vertices.
- **Graph:** Randomly sample  $N \in [4, 16]$  points. First, use Kruskal’s algorithm (Kruskal, 1956) to find a Minimum Spanning Tree that connects all the points. Then randomly add additional edges to the graph.

**Generation procedures (Composition):** Iteratively draw shapes on the canvas chosen from the following set of object types: [“circle”, “rectangle”, “triangle”, “line segment”]. After the first shape is drawn, at each iteration, the later shapes are constrained to have the same color as the previous shapes. We ensure overlap between the newly added shape and the previous shapes, while making sure that the intersection ratio does not exceed a predefined threshold. This prevents cases where one shape entirely contains another, making it impossible to decode into individual Primal Visual Description elements.

**PVD 160K dataset:** Using the aforementioned generation procedure, we generate a large-scale dataset containing 160K (SVG, PVD) pairs for training the LLM-based SVG-to-PVD model. The detailed configuration can be found in Table 3.

**Data augmentation details:** To enhance the robustness of the SVG-to-PVD model to images with various sizes and quality, we introduce the following randomized data augmentation during data generation.

- **Random pixel noise:** Probability (how often to apply the augmentation): 0.1; Ratio range (what portion of the selected area will be filled with noise pixels): (0.01, 0.05); Intensity range (the intensity of the noise pixels): (0.1, 1.0); Dilate range (how many pixels will the selection area be extended from the boundary): (1, 3) in pixels; Noise size: (1, 3) in pixels.
- **Gaussian blur:** Probability (how often to apply the augmentation): 0.1; Radius: (0.1, 0.5).

## D Full Response of the Example in Figure 2

See Figure 13 for the full input prompt and the generated response from GPT-4 on the  $2 \times 2$  maze-solving task shown in Figure 2.

## E Task Prompts

Figure 14 shows the prompts for models with image representations as visual inputs, i.e., GPT-4V, Llava, and ViperGPT.

Figures 15-22 show the prompts for VDLM, where `{perception}` will be filled with the aggregated Primal Visual Description perception result, and the `orange text` are instance-specific inputs such as the question. As mentioned in § 4.2, symbolic representations typically fail to retain visual inductive biases, necessitating additional clarifications to mitigate ambiguity in the tasks. For instance, in the Angle Classification task, more explicit instructions are provided regarding which angle the question is asking for. Another noteworthy point is that, in contrast to visual inputs that naturally accommodate a degree of imprecision, symbolic representations lack such inherent leniency. For instance, even if two line segments differ by only one pixel in length, they might be considered identical in visual representations, but symbolic representations would likely identify them as different. To reintroduce a level of tolerance in tasks that involve arithmetic reasoning, such as length comparison, we incorporate task-specific instructions to account for a reasonable margin of error, like 5%.

## F Newly Constructed Downstream Task Datasets

**Angle Classification.** We use the Geoclidian data generator<sup>11</sup> to generate images containing a single acute or obtuse angle with randomized orientations and ray lengths. The domain-specific language for generating the two concepts are shown as follows:

- Acute Angle:

```
"l1* = line(p1(), p2()),  
"c1* = circle(p1(), p2()),  
"c2* = circle(p2(), p1()),  
"l2* = line(p3(c1, c2), p4(c1, c2)),  
"l4 = line(p5(11, 12), p7(11)),  
"l5 = line(p6(12), p7(11))"
```

- Obtuse Angle:

```
"l1* = line(p1(), p2()),  
"c1* = circle(p1(), p2()),  
"c2* = circle(p2(), p1()),  
"l2* = line(p3(c1, c2), p4(c1, c2)),  
"l3* = line(p5(11, 12), p6(12)),  
"l4* = line(p5(11, 12), p7(11)),  
"l5* = line(p6(12), p7(11)),  
"l6* = line(p8(13, 14), p9(15)),  
"l100* = line(p5(c1, c2), p10(16)),  
"c101* = circle(p5(c1, c2), p10(16)),  
"c102* = circle(p10(16), p5(c1, c2)),  
"l101* = line(p100(c101, c102), p101(c101, c102)),  
"l7 = line(p11(1100, 1101), p6(12)),  
"l8 = line(p11(1100, 101), p7(11))"
```

<sup>11</sup> [https://github.com/joyhsu0504/geoclidian\\_framework](https://github.com/joyhsu0504/geoclidian_framework)

**Length Comparison.** We use matplotlib<sup>\*\*</sup> to plot two non-intersecting line segments on a canvas. These line segments may either be of identical length or of differing lengths. In scenarios where the lengths vary, we ensure the discrepancy is substantial (exceeding 15% relative to the length of the shorter line segment) to ensure perceptibility. The orientation of each line segment is determined independently and randomly, being either horizontal or vertical.

**Maze Solving.** We leverage the maze-dataset package<sup>††</sup> to generate 2D unsolved mazes along with their corresponding ground truth solutions. We use “circle” shape to denote the start position and “star” shape to denote the end position. We generate two subsets featuring  $2 \times 2$  and  $3 \times 3$  maze configurations.

## G Dataset Statistics

		# Training Instances	# Eval Instances
Probing Tasks	Line or Angle	10K	1K
	Angle Classification	10K	1000
	Length Comparison	10K	1000
	Clevr QA	36K	1000
	Shapeworld Scene	15K	100
	Maze Scene	10K	600
Zero-Shot Downstream Tasks	Angle Classification		
	Length Comparison	-	100
	Shapeworld Spatial Reasoning (2Obj)	-	100
	Shapeworld Spatial Reasoning (MultiObj)	-	100
	Shapeworld Superlative	-	100
	NLVR	-	100
	Geoclidean 2-shot Learning	-	100
	$2 \times 2$ Maze Solving	-	100
	$3 \times 3$ Maze Solving	-	100

Table 4: Statistics of the probing tasks (§ A.1) and the downstream tasks (§ 3). The GPT-4(V) zero-shot results on probing tasks are reported on 100 randomly sub-sampled instances from the entire eval split.

Detailed statistics of the probing tasks used in § A and the zero-shot downstream tasks mentioned in § 3 can be found in Table 4.

<sup>\*\*</sup><https://matplotlib.org/stable/>

<sup>††</sup><https://github.com/understanding-search/maze-dataset/tree/main>

**Input Prompt**

The following JSON contains an approximated perception of a 2x2 maze. Each object (potentially including the background) is represented by a list of geometric shapes. If the object contains multiple shapes, it is a composite object. The (x, y) coordinates for the vertices and edges correspond to the width and height position in pixels, and (0, 0) is the top-left corner of the image.

```

--- perception ---
[{"object_0": [{"type": "rectangle", "vertices": [[0, 0, 336.0], [0, 0, 0], [336.0, 0, 0], [336.0, 336.0]], "color": [253, 253, 253], "style": "filled shape"}], "object_1": [{"type": "grid", "vertices": [[16, 16], [16, 164], [16, 312], [172, 16], [172, 164], [172, 312], [328, 16], [328, 164], [328, 312]], "edges": [[[16, 16], [16, 164]], [[16, 16], [172, 16]], [[16, 164], [16, 312]], [[16, 164], [172, 164]], [[172, 16], [172, 164]], [[172, 16], [172, 312]], [[172, 164], [172, 312]], [[328, 16], [328, 164]], [[328, 16], [328, 312]], [[328, 164], [328, 312]]], "color": [0, 0, 0], "line_width": 10}], "object_2": [{"type": "circle", "center": [94, 94], "radius": 14, "color": [255, 4, 4], "style": "filled shape"}], "object_3": [{"type": "triangle", "vertices": [[242, 221], [231, 259], [250, 236]], "color": [255, 7, 7], "style": "filled shape"}]}
-----
```

In the 2x2 maze, walls are depicted by a grid of black lines between cells and along the perimeter. The maze cells are defined within the grid. The start position is marked by a red circle, and the end position by a red star. The position of each cell can be represented by coordinates (row, column), beginning from the top-left corner as (0, 0). Here, 'row' corresponds to the vertical dimension (height) of the image, and 'column' to the horizontal dimension (width).

Perform the following steps to solve the maze:

- (1) Infer the connectivity of the cells using a connection list. For example, a 2x2 maze should have a 'connection\_list' containing two sublists with dimension 1x2 and 2x1. For  $i$  in  $\text{range}(0, 1)$  and  $j$  in  $\text{range}(0, 2)$ ,  $\text{connection\_list}[0][i][j]$  is 'True' if cell '(i, j)' is vertically connected to cell '(i+1, j)' without being separated by a wall. Similarly, for  $j$  in  $\text{range}(0, 1)$  and  $i$  in  $\text{range}(0, 2)$ ,  $\text{connection\_list}[1][i][j]$  is 'True' if cell '(i, j)' is horizontally connected to cell '(i, j+1)' without being separated by a wall.
- (2) Infer the start position and end position of the maze in the row-column format.
- (3) Solve the maze by finding a path from the start position to the end position.

You MUST provide your final answer, and the answer should follow this format: {"solution": "a list of (row, column) coordinates"}

**GPT-4 Response**

To solve the maze based on the provided JSON data, let's break down the steps as required:

**## Step 1: Infer the Connectivity of the Cells**

Given the grid lines and their coordinates, we can infer the connectivity between cells. **The grid lines form the boundaries of a 2x2 maze, meaning there are 3 vertical lines and 3 horizontal lines that define the cells. By examining the edges in the JSON, we can determine where the walls are and thus infer which cells are connected.**

- Vertical connections ('connection\_list[0]'): There are no vertical walls inside the maze, so both cells in the first column are connected to their respective cells in the second column.
- Horizontal connections ('connection\_list[1]'): There is a horizontal wall between the two cells in the first row, meaning there's no direct connection between them. However, the cells in the second row are connected.

Therefore, the 'connection\_list' can be represented as:

- Vertical connections: "[[True, True]]"
- Horizontal connections: "[[False], [True]]"

**## Step 2: Infer the Start and End Positions**

- The start position is marked by a red circle, which is located at approximately '(94, 94)'. This places it in the **top-left cell, or (0, 0)**.
- The end position is marked by a composite red shape resembling a star, located in the **bottom-right cell**, which can be inferred from the coordinates of the triangles forming the star shape. This places the end position at '(1, 1)'.

**## Step 3: Solve the Maze**

Given the connectivity and the start/end positions, we can find a path from the start to the end. The path, considering the connectivity and the positions, would be:

1. Start at '(0, 0)'.
2. Move right to '(0, 1)'.
3. Move down to '(1, 1)'.

Thus, the solution path is: '[(0, 0), (0, 1), (1, 1)]'.

**## Final Answer**

```

...json
{"solution": "[(0, 0), (0, 1), (1, 1)]"}

```

Figure 13: Full input prompt and GPT-4 response of the 2x2 maze solving example in Figure 2. The **blue** part in the input prompt indicates the generated Primal Visual Description (PVD) of the entire image.

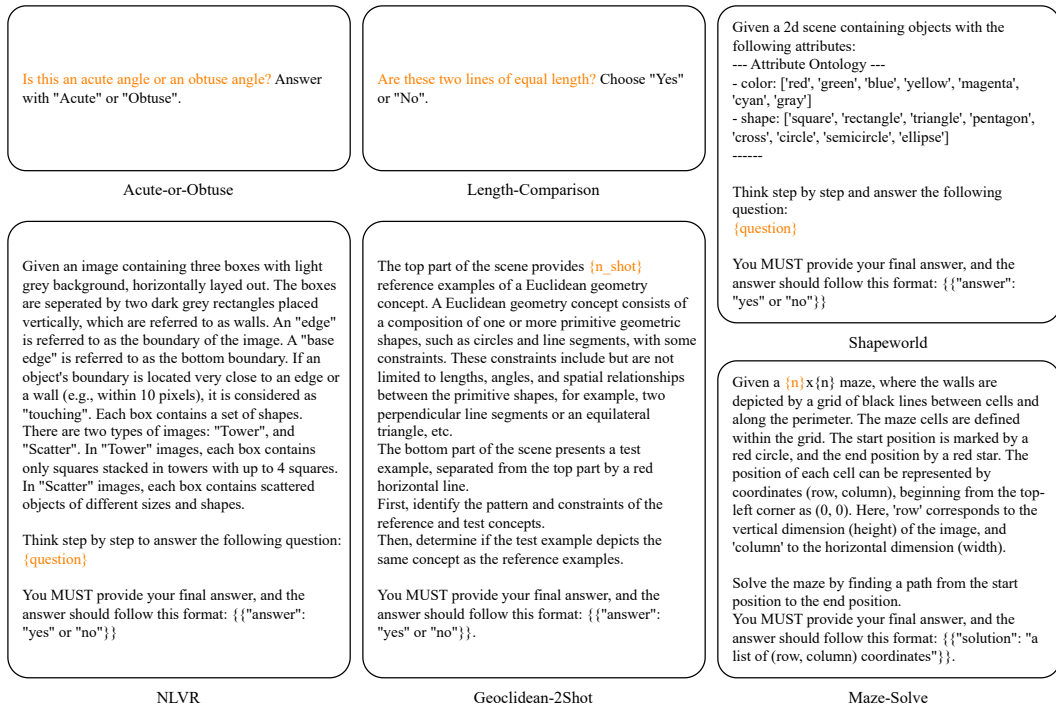


Figure 14: Prompts for zero-shot downstream tasks with image input

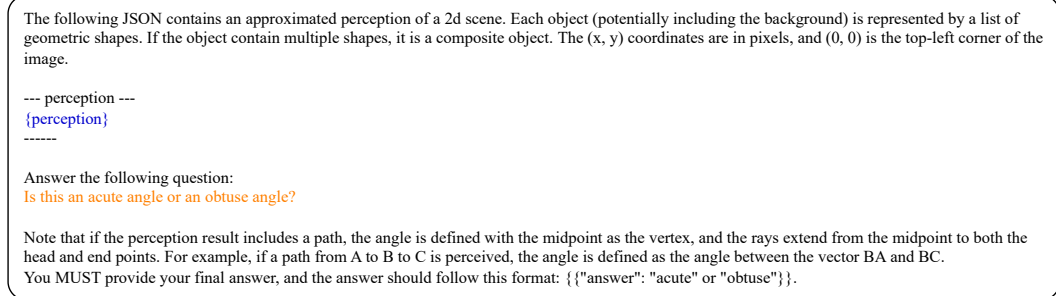


Figure 15: Prompt for task Angle Classification with Primal Visual Description perception input.

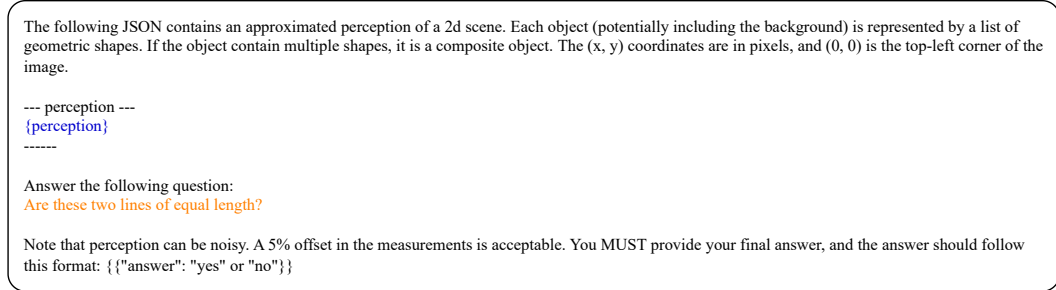


Figure 16: Prompt for task Length Comparison with Primal Visual Description perception input.

Given a 2d scene containing objects with the following attributes:

--- Attribute Ontology ---  
- color: ['red', 'green', 'blue', 'yellow', 'magenta', 'cyan', 'gray']  
- shape: ['square', 'rectangle', 'triangle', 'pentagon', 'cross', 'circle', 'semicircle', 'ellipse']  
-----

The following JSON contains an approximated perception of the scene. Each object (potentially including the background) is represented by a list of geometric shapes. If the object contain multiple shapes, it is a composite object. The (x, y) coordinates are in pixels, and (0, 0) is the top-left corner of the image.

--- perception ---  
{perception}  
-----

Note that the perception can be noisy. First identify the best matching shape type and the color type from the ontology for each perceived object. For composite objects, please match the entire composition to one of the most probable objects in the ontology. Make educated guesses if necessary. Then, think step by step and answer the following question:

{question}

You MUST provide your final answer, and the answer should follow this format: {{"answer": "yes" or "no"}}}

Figure 17: Prompt for task Shapeworld Spatial Reasoning (2Obj) with Primal Visual Description perception input.

Given a 2d scene containing objects with the following attributes:

--- Attribute Ontology ---  
- color: ['red', 'green', 'blue', 'yellow', 'magenta', 'cyan', 'gray']  
- shape: ['square', 'rectangle', 'triangle', 'pentagon', 'cross', 'circle', 'semicircle', 'ellipse']  
-----

The following JSON contains an approximated perception of the scene. Each object (potentially including the background) is represented by a list of geometric shapes. If the object contain multiple shapes, it is a composite object. The (x, y) coordinates are in pixels, and (0, 0) is the top-left corner of the image. If two objects overlap, the one with the larger index is considered to be in front of the other.

--- perception ---  
{perception}  
-----

Note that the perception can be noisy. First identify the best matching shape type and the color type from the ontology for each perceived object. For composite objects, please match the entire composition to one of the most probable objects in the ontology. Make educated guesses if necessary. Then, think step by step and answer the following question:

{question}

You MUST provide your final answer, and the answer should follow this format: {{"answer": "yes" or "no"}}}

Figure 18: Prompt for task Shapeworld Spatial Reasoning (MultiObj) with Primal Visual Description perception input.

Given a 2d scene containing objects with the following attributes:

--- Attribute Ontology ---  
- color: ['red', 'green', 'blue', 'yellow', 'magenta', 'cyan', 'gray']  
- shape: ['square', 'rectangle', 'triangle', 'pentagon', 'cross', 'circle', 'semicircle', 'ellipse']  
-----

The following JSON contains an approximated perception of the scene. Each object (potentially including the background) is represented by a list of geometric shapes. If the object contain multiple shapes, it is a composite object. The (x, y) coordinates are in pixels, and (0, 0) is the top-left corner of the image. The lowermost object has the largest y-coordinate, and the rightmost object has the largest x-coordinate.

--- perception ---  
{perception}  
-----

Note that the perception can be noisy. First identify the best matching shape type and the color type from the ontology for each perceived object. For composite objects, please match the entire composition to one of the most probable objects in the ontology. Make educated guesses if necessary. Then, think step by step and answer the following question:

{question}

You MUST provide your final answer, and the answer should follow this format: {{"answer": "yes" or "no"}}}

Figure 19: Prompt for task Shapeworld Superlative with Primal Visual Description perception input.

Given an image containing three boxes with light grey background, horizontally laid out. The boxes are separated by two dark grey rectangles placed vertically, which are referred to as walls. An "edge" is referred to as the boundary of the image. A "base edge" is referred to as the bottom boundary. If an object's boundary is located very close to an edge or a wall (e.g., within 10 pixels), it is considered as "touching". Each box contains a set of shapes. There are two types of images: "Tower", and "Scatter". In "Tower" images, each box contains only squares stacked in towers with up to 4 squares. In "Scatter" images, each box contains scattered objects of different sizes and shapes.

The following JSON contains an approximated perception of the image. Each object (potentially including the background) is represented by a list of geometric shapes. If the object contain multiple shapes, it is a composite object. The (x, y) coordinates are in pixels, and (0, 0) is the top-left corner of the image.

```
--- perception ---
{perception}
-----
```

Now, identify the content in each box based on the perception result, and then think step by step to answer the following question:

```
{question}
```

You MUST provide your final answer, and the answer should follow this format: `{"answer": "yes" or "no"}`

Figure 20: Prompt for task NLVR with Primal Visual Description perception input.

The following JSON contains an approximated perception of the image. Each object (potentially including the background) is represented by a list of geometric shapes. If the object contain multiple shapes, it is a composite object. The (x, y) coordinates are in pixels, and (0, 0) is the top-left corner of the image.

```
--- perception ---
{perception}
-----
```

The top part of the scene provides `{n shot}` reference examples of a Euclidean geometry concept. A Euclidean geometry concept consists of a composition of one or more primitive geometric shapes, such as circles and line segments, with some constraints. These constraints include but are not limited to lengths, angles, and spatial relationships between the primitive shapes, for example, two perpendicular line segments or an equilateral triangle, etc.

The bottom part of the scene presents a test example, separated from the top part by a red horizontal line.

First, identify the pattern and constraints of the reference and test concepts based on the perception result. Note that the perception can be noisy. Make educated guesses if necessary.

Then, determine if the test example depicts the same concept as the reference examples.

You MUST provide your final answer, and the answer should follow this format: `{"answer": "yes" or "no"}`.

Figure 21: Prompt for task Geoclidian 2-shot Learning with Primal Visual Description perception input.

The following JSON contains an approximated perception of a `{n}x{m}` maze. Each object (potentially including the background) is represented by a list of geometric shapes. If the object contains multiple shapes, it is a composite object. The (x, y) coordinates for the vertices and edges correspond to the width and height position in pixels, and (0, 0) is the top-left corner of the image.

```
--- perception ---
{perception}
-----
```

In the `{n}x{m}` maze, walls are depicted by a grid of black lines between cells and along the perimeter. The maze cells are defined within the grid. The start position is marked by a red circle, and the end position by a red star. The position of each cell can be represented by coordinates (row, column), beginning from the top-left corner as (0, 0). Here, 'row' corresponds to the vertical dimension (height) of the image, and 'column' to the horizontal dimension (width).

Perform the following steps to solve the maze:

- (1) Infer the connectivity of the cells using a connection list. For example, a `{n}x{m}` maze should have a 'connection\_list' containing two sublists with dimension `{m}x{n}` and `{n}x{m}`. For  $i$  in  $\text{range}(0, \{m\})$  and  $j$  in  $\text{range}(0, \{n\})$ , 'connection\_list[0][i][j]' is 'True' if cell '(i, j)' is vertically connected to cell '(i+1, j)' without being separated by a wall. Similarly, for  $j$  in  $\text{range}(0, \{m\})$  and  $i$  in  $\text{range}(0, \{n\})$ , 'connection\_list[1][i][j]' is 'True' if cell '(i, j)' is horizontally connected to cell '(i, j+1)' without being separated by a wall.
- (2) Infer the start position and end position of the maze in the row-column format.
- (3) Solve the maze by finding a path from the start position to the end position.

You MUST provide your final answer, and the answer should follow this format: `{"solution": "a list of (row, column) coordinates"}`.

Figure 22: Prompt for task Maze Solving with Primal Visual Description perception input.